NeuroImage: Clinical 23 (2019) 101816

Contents lists available at ScienceDirect

NeuroImage: Clinical

journal homepage: www.elsevier.com/locate/ynicl

Electroconvulsive therapy "corrects" the neural architecture of visuospatial memory: Implications for typical cognitive-affective functioning

Raluca Petrican[a,*,1], Hedvig Söderlund[b,1], Namita Kumar[c], Zafiris J. Daskalakis[d,f], Alastair Flint[e,f], Brian Levine[g,*]

[a] Rotman Research Institute, Canada
[b] Uppsala University, Sweden
[c] Baycrest Centre for Geriatric Care, Toronto, Ontario, Canada
[d] Centre for Addiction and Mental Health, Clarke Division,Toronto, Ontario, Canada
[e] University Health Network, Toronto, Ontario, Canada
[f] University of Toronto, Canada
[g] Rotman Research Institute, University of Toronto, Canada

ARTICLE INFO

Keywords:
Depression
Electroconvulsive therapy
Autobiographical memory
Functional networks
Genes

ABSTRACT

Although electroconvulsive therapy (ECT) is a widely used and effective treatment for refractory depression, the neural underpinnings of its therapeutic effects remain poorly understood. To address this issue, here, we focused on a core cognitive deficit associated with depression, which tends to be reliably ameliorated through ECT, specifically, the ability to learn visuospatial information. Thus, we pursued three goals. First, we tested whether ECT can "normalize" the functional brain organization patterns associated with visuospatial memory and whether such corrections would predict post-ECT improvements in learning visuospatial information. Second, we investigated whether, among healthy individuals, stronger expression of the neural pattern, susceptible to adjustments through ECT, would predict reduced incidence of depression-relevant cognition and affect. Third, we sought to quantify the heritability of the ECT-correctable neural profile. Thus, in a task fMRI study with a clinical and a healthy comparison sample, we characterized two functional connectome patterns: one that typifies trait depression (i.e., differentiates patients from healthy individuals) and another that is susceptible to "normalization" through ECT. Both before and after ECT, greater expression of the trait depression neural profile was associated with more frequent repetitive thinking about past personal events (affective persistence), a hallmark of depressogenic cognition. Complementarily, post-treatment, stronger expression of the ECT-corrected neural profile was linked to improvements in visuospatial learning, a mental ability which is markedly impaired in depression. Subsequently, using data from the Human Connectome Project (HCP) (N = 333), we demonstrated that the functional brain organization of healthy participants with greater levels of subclinical depression and higher incidence of its associated cognitive deficits (affective persistence, impaired learning) shows greater similarity to the trait depression neural profile and reduced similarity to the ECT-correctable neural profile, as identified in the patient sample. These results tended to be specific to learning-relevant task contexts (working memory, perceptual relational processing). Genetic analyses based on HCP twin data (N = 128 pairs) suggested that, among healthy individuals, a functional brain organization similar to the one normalized by ECT in the patient sample is endogenous to cognitive contexts that require visuospatial processing that extends beyond the here-and-now. Broadly, the present findings supported our hypothesis that some of the therapeutic effects of ECT may be due to its correcting the expression of a naturally occurring pattern of functional brain organization that facilitates integration of internal and external cognition beyond the immediate present. Given their substantial susceptibility to both genetic and environmental effects, such mechanisms may be useful both for identifying at risk individuals and for monitoring progress of interventions targeting mood-related pathology.

Electroconvulsive therapy (ECT) is a widely used and effective treatment for refractory depression, whose therapeutic effects have

* Corresponding authors at: Rotman Research Institute, 3560 Bathurst Street, Toronto, Ontario M6A 2E1, Canada.
E-mail addresses: rpetrican@research.baycrest.org (R. Petrican), blevine@research.baycrest.org (B. Levine).
[1] R.P. and H.S. are co-first authors.

https://doi.org/10.1016/j.nicl.2019.101816
Received 14 February 2019; Received in revised form 25 March 2019; Accepted 3 April 2019
Available online 05 April 2019

been linked to seizure-induced systems-level reorganization of functional neural connections (Farzan et al., 2017; Husain et al., 2004; Semkovska and McLoughlin, 2010). Nonetheless, the specific brain substrates underlying its beneficial effects remain to be elucidated (but see Dukart et al., 2014). To address this question, here, we focused on a core cognitive deficit associated with depression, which tends to be reliably ameliorated through ECT, specifically, the ability to learn visuospatial information (Mohn and Rund, 2016; Semkovska and McLoughlin, 2010). Our goal was two-fold. First, we sought to shed light on whether ECT has a unique positive effect on the brain architecture associated with visuospatial memory, which, in turn, predicts post-ECT behavioral improvements in visuospatial learning. Second, we intended to elucidate whether, in the healthy population, the aforementioned neural profile, susceptible to ECT-induced "corrections", would predict reduced incidence of depression-related mentation and affect. This line of investigation could further our understanding of the neurocognitive markers of depression vulnerability, as well as point to viable intervention targets for at-risk individuals.

To test these hypotheses, we leveraged pre−/post-treatment fMRI data from a sample of patients with severe depression who underwent ECT. Our analyses focused on a cued episodic autobiographical memory task, in which participants were specifically asked to visualize past personal events (i.e., the people, objects and spatial layout associated with each cued event). This was contrasted to a simple number judgment task that relies on non-episodic and, most likely, non-visual processes. Our primary goal was to elucidate whether ECT would uniquely "correct" the patients' functional brain architecture in the autobiographical memory condition (i.e., make the patients' functional architecture more similar to that of controls in this task). Autobiographical memory recall draws heavily on visual processing resources (e.g., Daselaar et al., 2008; Greenberg et al., 2005; Vannucci et al., 2016) and our task specifically required participants to access the visuospatial details of the cued episodes. Consequently, we reasoned that patients' stronger expression of the "corrected" brain profile, specific to the autobiographical memory task, would predict improvements in how they process (i.e., perceive and subsequently remember) visuospatial information. To test this hypothesis, we focused on a task that assesses learning for visuospatial information acquired post-ECT because access to information acquired pre-ECT is generally impaired (i.e., retrograde amnesia, cf. Sackeim, 2014; Semkovska and McLoughlin, 2014). This is assumed to occur because ECT accelerates neurogenesis and the ensuing systems level functional reorganization disrupts access to previously acquired memories (Farzan et al., 2017; Frankland and Josselyn, 2016). Our secondary goal was to characterize the neural profile associated with trait depression, specifically, the one that differentiates patients from healthy comparison individuals, both before and after ECT.

We then tested whether, among unrelated healthy young adults from the Human Connectome Project (HCP), variations in subclinical depression could be predicted from how similar an individual's functional brain organization was to the neural profile associated with trait depression versus the neural profile, susceptible to "correction" through ECT, as identified in the patient data. Functional brain organization in the HCP sample was characterized during eight task conditions (Barch et al., 2013). Our hypotheses focused on the four task conditions (i.e., online maintenance versus updating of mental representations, static versus dynamic relational processing) that assess mental processes relevant to visuospatial learning and episodic autobiographical memory, particularly as tested in the ECT sample (i.e., by emphasizing visualization; see Palombo, Sheldon, & Levine, 2018, for the unique role of visualization in episodic autobiographical memory, in general). Of these, two were derived from a working memory task and focused on processes relevant to online maintenance of mental representations, whereas the other two focused on perceptual relational processing (i.e., static versus dynamic). The remaining four task conditions were only introduced to test the contextual specificity of our observed brain-behavior relationships, given recent evidence of substantial cross-task overlap in functional brain architecture (Gratton et al., 2018). Finally, we employed a sample of identical versus fraternal twins from HCP to quantify the relative contribution of genetic versus environmental factors to the similarity between an individual's functional brain organization during the aforementioned mnemonically relevant task conditions (i.e., online maintenance versus perceptual relational processing) and the neural profiles identified in the patient data.

As noted above, we probed the ability to encode and mentally manipulate visual information, a key depressogenic deficit (Baune et al., 2014; Zakzanis et al., 1998). This cognitive facet constituted a primary outcome in the ECT sample in which it was assessed with a visuospatial learning task. In the HCP sample, encoding and mental manipulation of visual information was assessed with a list sorting task.

The second cognitive aspect scrutinized was the predisposition towards thinking repetitively about prior personal episodes, presumably indicative of a broader tendency to "latch on" to affectively laden self-relevant information (Watkins and Nolen-Hoeksema, 2014; Whitmer and Gotlib, 2013). In the ECT sample, this aspect was operationalized as the self-reported frequency of thinking about past personal episodes. In the HCP sample, it was operationalized as valuation of delayed rewards, a proxy for the affective persistence of motivationally relevant stimuli. The positive conceptualization of this depressogenic cognitive tendency dovetails prior evidence linking it to better focus on goal-relevant information among non-depressed individuals (Whitmer and Gotlib, 2013).

The present report is organized as follows. Part 1 focuses on the ECT sample and details the identification and behavioral relevance of the functional brain organization patterns linked to trait depression versus those that are "corrected" by ECT. Part 2 focuses on a sample of unrelated individuals from the HCP (HCP Sample 1) with the goal of determining whether the functional brain organization patterns, identified in Part 1, can be used to predict subclinical variations in depression and its associated cognitive deficits. Part 3 focuses on a sample of identical and fraternal twins from the HCP (HCP Sample 2) in order to establish the heritability of the functional brain organization patterns described in Part 1.

Across all samples herein scrutinized, whole brain functional organization for each participant within each task context (i.e., episodic memory versus number judgment in the ECT sample; cognitive versus social-affective context in the HCP samples) was estimated with graph theoretical tools. In Part 1, we identified differences in whole brain functional organization between task contexts, as well as between depressed patients and comparison participants by employing partial least squares analysis (PLS), a powerful multivariate technique, sensitive enough to use with sample sizes even smaller than ours (cf. McIntosh and Lobaugh, 2004), which can detect in an unconstrained, data-driven manner patterns of functional brain organization which differ as a function of experimental conditions and/or groups. In Parts 2 and 3, the similarity between each individual's functional brain organization in each task context and the trait depression versus the ECT-correctable neural profile was quantified by using the PLS weights corresponding to each of these two brain patterns, as identified in Part 1. In Part 2, we used canonical correlation analysis to determine whether similarity between an individual's functional brain organization and the trait depression versus the ECT-correctable neural profile predicts his or her level of subclinical depression and associated cognitive deficits (impaired learning, affective persistence). In Part 3, we employed structural equation modelling to quantify genetic versus environmental contributions to the similarity between an individual's functional brain organization and the trait depression versus the ECT-correctable neural profile, as identified in Part 1.

1. Part 1: ECT sample

1.1. Method

1.1.1. Participants

Ten healthy, right-handed controls (33.10 ± 8.02 years old; 15.50 ± 2.99 years of education; four men) and fifteen severely depressed patients (47.13 ± 13.26 years old; 14.97 ± 3.43 years of education; four men; one left-handed), referred for electroconvulsive therapy (ECT), participated in the study. The controls were part of the Rotman Research Institute participant pool. The patients were recruited from psychiatric clinics affiliated with the University of Toronto. All participants were screened for a history of severe neurological conditions, as well as for physical conditions or bodily implants that may render their participation unsafe. Participants provided informed consent in accordance with the research ethics board at the Rotman Research Institute.

For the controls, lack of a psychiatric diagnosis was confirmed by administering the Structured Clinical Interview for the Diagnostic and Statistical Manual of Mental Disorders, 4th edition (SCID; First, Spitzer, Williams, & Gibbon, 1995). For the patients, clinical diagnosis was made by the treating psychiatrist who recommended the ECT and confirmed with the SCID. Both before and after ECT, all patients were on a medication schedule consonant with their diagnosis (see Table 1). Twelve patients had a diagnosis of major depressive disorder, two had a diagnosis of bipolar I disorder and one had a diagnosis of schizoaffective disorder with depression. Tables 1 and S1 contain a full description of the demographic and clinical characteristics of the ECT sample.

1.1.1.1. Core patient sample. To increase the reliability of the identified functional connectivity patterns, the analyses aimed at differentiating the autobiographical memory from the general task architecture in patients versus controls included only the ten patients who complied with the study demands (see Tables 1 and S1 for the demographic and clinical characteristics of this subsample). Specifically, these ten patients (1) completed all four functional runs; (2) demonstrated good understanding of the two in-scanner tasks and (3) generated at least 29 of the 40 requested events, evenly spread out across the four time periods under scrutiny (see below for details). This filtering was done in order to ensure that any differences between patients and controls reflect differences in how the two groups perform the same tasks, rather than the fact that the two groups perform somewhat different tasks due to lack of understanding and/or compliance. All ten patients from the core sample had a diagnosis of major depressive disorder, making it a fairly homogenous sample. Data from all fifteen patients were entered in the brain-behavior analyses involving neuropsychological test performance and affective/motivational persistence of the recalled autobiographical events (see Method below for details).

1.1.2. Procedure

1.1.2.1. ECT. ECT was administered with a spECTrum 5000Q device (MECTA Corporation) according to standards of practice (Sackeim et al., 2008). Treatment sessions occurred twice or three times per week and were continued until depressive symptoms were in remission or improvement had plateaued. Information on ECT type (right unilateral/bilateral) and number of sessions is included in Tables 1 and S1. Because number of ECT treatments was determined by ongoing clinical evaluation, it varied across patients (cf. Farzan et al., 2017). Nonetheless, we verified that number of ECT treatments was not significantly related to any of the cognitive or brain variables herein scrutinized (all *ps* > .27).

Seizure threshold was individually determined by the administration of repeated stimuli of increasing intensity until a generalized seizure occurred. Stimulus intensity was generally set at 5 times the seizure threshold for unilateral ECT and 3 times the seizure threshold for bilateral ECT. The intensity was further elevated if there was an absence of seizures or their intensity was clinically judged inadequate.

Table 1
Demographic and clinical characteristics of the patient and control ECT sample.

	Patients (N = 15)	Patients^{main} (N = 10)	Controls (N = 10)
Age (yrs)	47.13 ± 13.26	44.30 ± 12.41*	33.10 ± 8.02
Education (yrs)	14.97 ± 3.43	14.80 ± 3.58	15.50 ± 2.99
Sex (men/women)	4/11	3/7	4/6
Session 1-ECT start (days)	6.36 ± 5.76	7.56 ± 6.48	N/A
Session 1-Session 2 (days)	121.27 ± 49.23***	112.80 ± 53.86*	61.00 ± 17.23
ECT end-Session 2 (days)	69.21 ± 40.11	63.56 ± 46.90	N/A
Time since diagnosis (yrs)	12.30 ± 9.08	12.35 ± 9.23	N/A
Number of ECT treatments	11.93 ± 6.23	11.50 ± 6.36	N/A
Number of bilateral ECT treatments	7.57 ± 5.26	7.67 ± 5.45	N/A
Number of unilateral ECT treatments	5.00 ± 4.92	4.78 ± 4.15	N/A
Antidepressants (% patients)	93	100	N/A
Mood stabilizers (% patients)	36	33	N/A
Atypical antipsychotics (% patients)	36	22	N/A
Benzodiazepines (% patients)	57	67	N/A
BDI Score-Session 1	36.47 ± 9.22$_a$	35.40 ± 11.14$_a$	N/A
BDI Score-Session 2	27.80 ± 11.74$_b$	24.30 ± 12.54$_b$	N/A
BVMT-R -Session 1	24.93 ± 6.22	27.00 ± 4.81	N/A
BVMT-R -Session 2	23.13 ± 7.76	26.80 ± 6.37	N/A
Events-last week	8.40 ± 2.10*	8.90 ± 1.91	10
Events-last month	8.27 ± 1.91**	8.70 ± 1.70*	10
Events-last year	8.67 ± 1.96*	9.50 ± 1.27	10
Events-last decade	8.27 ± 2.71*	9.50 ± .97	10

Note. Patients were on the same medication type both before and after ECT. Different subscripts (a/b) indicate statistically significant differences between Session 1 and Session 2 scores, as revealed by paired-samples *t*-tests for a p-value < .05.

* Patients differed from controls at p < .05.

** Patients differed from controls at p < .01.

*** Patients differed from controls at p < .001. Patients^{main} constituted the group of 10 patients included in the multivariate analyses aimed at differentiating the autobiographical memory from the general task architecture in patients versus controls at Time 1 (pre-ECT for patients) versus Time 2 (post-ECT for patients). BDI = Beck Depression Inventory. BVMT-R = Brief Visuospatial Memory Test–Revised.

Methohexital, penthotal, thiopental or thiopentone was administered for sedation and succinylcholine as neuromuscular blocker.

1.1.2.2. fMRI study. A few days prior to their first fMRI appointment, participants generated a list of autobiographical events (see below for details). Subsequently, the entire sample took part in two fMRI sessions, approximately four months apart (see Table 1 for details). For the patients, the first appointment preceded the start of their ECT treatment, whereas the second appointment took place approximately two months after their last ECT session (see Table 1). On both occasions, participants completed a series of out-of-scanner and in-scanner tasks, as described below.

1.1.3. Cognitive-affective measures (out-of-scanner)

1.1.3.1. Autobiographical memory

1.1.3.1.1. Event identification. Prior to their first fMRI appointment, participants dated and gave titles to 40 autobiographical events, 10 from each of the following time periods: the last week (14 days, excluding the last 2 days); the last month (3–7 weeks); the last year (6–18 months) and the last 10 years (5–10 years) (see Table 1 for a comparison between controls and patients with respect to the number of events generated for each period). Time periods were presented as ranges to allow for sufficient events to be generated across all participants. Participants were instructed to provide events that were specific to a single space and took no longer than a day to unfold. To maximize comparability of recall during the first versus the second fMRI appointment, participants were instructed to identify events that comprised two distinguishable episodes and provide a title for each constituent episode (e.g., "My daughter's wedding", Part 1: "Wedding ceremony", Part 2: "Wedding reception"). Thus, for each event, one component was cued during the first fMRI appointment, whereas the second component was cued during the second fMRI appointment.

1.1.3.1.2. Event ratings: affective persistence. After their first scanning session, participants used a six-point scale to rate each event on five control dimensions: visualization, emotional valence, emotional change at the time of the event, importance at the time the event occurred and present day importance of the event. Our dimension of interest, frequency of thinking or talking about the event, which we regarded as a proxy for its affective persistence, was measured on a 12-point scale, ranging from 0 (*never*) to 11 (*constantly*).

1.1.3.2. Visuospatial leaning. Before and after ECT, visuospatial learning was assessed with the Brief Visuospatial Memory Test–Revised (BVMT-R, Benedict, 1997). Alternate forms were administered to minimize practice effects. A change score in visuospatial learning from before to after ECT was computed by regressing the post-ECT BVMT total score onto the corresponding pre-ECT score. At the whole-group level, a paired samples *t*-test revealed no statistically significant changes in visuospatial learning, $t(14) = 1.102$, $p = .289$, although there was a statistically significant reduction in BDI scores, $t(14) = 2.894$, $p = .012$ (see Table 1).

The BVMT-R was part of a comprehensive test battery, which also gauged verbal learning (Hopkins Verbal Learning Test–Revised, Benedict et al., 1998) and speeded attention/information processing (Trail Making Test, Parts A and B, Army Individual Test Battery, the Symbol Digit Modalities Test, Smith, 1982, and verbal fluency). Nonetheless, because our hypotheses focused on visuospatial learning, for which, in the context of the present fMRI test paradigm, we expected the strongest effects, these additional tasks are not discussed in the present report. None of these additional measures showed statistically significant associations with any of the functional brain organization patterns herein documented (all $ps > .20$).

1.1.4. fMRI tasks

Both fMRI sessions comprised four functional runs. Each run lasted ~11 min and contained 10 autobiographical memory and 10 odd/even number judgment trials (cf. Söderlund et al., 2012). For the autobiographical memory task, within each run, two of the scrutinized time periods were featured with two events each, whereas the remaining periods were featured with three events each. For each participant, within each run, the presentation order of the two tasks and of the time periods for the autobiographical memory trials was randomized. Prior to testing, participants practiced both tasks outside the scanner.

1.1.4.1. Autobiographical memory. A trial began with a 1 s fixation, followed by a 4 s cue identifying the upcoming task ("Autobiographical memory"). Subsequently, participants saw one of their autobiographical memory titles for 18 s. During this period, they were asked to re-experience the event as vividly as possible, trying to recall associated thoughts, feelings and visual images. Next, participants were allowed 8 s to rate the degree to which they re-experienced the event. Ratings were made on an 8-point scale via fMRI-compatible response boxes.

1.1.4.2. Odd/even number judgment. A trial began with a 1 s fixation, followed by a 4 s cue identifying the upcoming task ("Odd/Even?"). Next, participants saw 9 numbers, presented one at a time for 1900 ms, each followed by a 100 ms interstimulus interval. They had to decide whether each number was odd or even without making an overt response. After the presentation of the last number in the trial, participants were allowed 8 s to rate on an 8-point scale the amount of re-experiencing of any past personal events. This rating was intended as a control for the degree to which participants did not focus on the task at hand, but instead allowed their minds to wander off to personally relevant information.

1.1.5. fMRI data acquisition

Images were acquired with a 3.0 T (Siemens Magnetom Trio Tim, Numaris/4Syngo MR B13; Siemens, Germany) with a 12-channel birdcage head coil. T1-weighted anatomical scans were acquired with a MP-RAGE sequence (TR = 2000 ms, TE = 2.63 ms, FOV = 256 mm, 256 × 256 matrix, 176 coronal slices of 1 mm isotropic voxels, perpendicular to the hippocampus). The high-resolution structural scan preceded the acquisition of functional scans.

Functional images were acquired over four runs with a single-shot T2-weighted pulse with spiral in/out (TR = 2000 ms, TE = 30 ms, flip angle = 70°, FOV = 200 mm, 64 × 64 matrix, 32 coronal slices, perpendicular to the hippocampus, of 3.1 × 3.1 mm in-plane resolution, 5 mm thick, no gap). To allow magnetization to reach equilibrium, the presentation of the task stimuli, described above, was delayed by 20 s from the start of each functional run. Details on the duration of each task condition, used in the connectivity analyses, are included in the section on fMRI data analysis.

1.1.6. fMRI data Preprocessing

We performed image processing in SPM12 (Wellcome Department of Imaging Neuroscience, London, UK). Specifically, we corrected for slice timing differences and rigid body motion (which included unwarping), spatially normalized the images to the standard Montreal Neurological Institute (MNI)-152 template, and smoothed them (full-width half-maximum, 6 mm).

Because motion can significantly impact functional connectivity measures (Power et al., 2012; Van Dijk et al., 2012), we implemented several additional preprocessing steps to address this potential confound. First, after extracting the BOLD time series from our regions-of-interest (ROIs, see below), but prior to computing the ROI-to-ROI correlations, we used the Denoising step in the CONN toolbox (version 17c; Whitfield-Gabrieli and Nieto-Castanon, 2012) to apply further physiological and rigid motion corrections. Specifically, linear regression was used to remove from the BOLD time series of each ROI the BOLD time series of the voxels within the MNI-152 white matter and CSF masks, respectively (i.e., the default CONN option of five CompCor-extracted

principal components for each, Behzadi, Restom, Liau, & Liu, 2007), a method for removing both physiological (e.g., breathing, pulse-related) and rigid motion effects, which is, at least as effective as those based on actual respiration and pulse measures (e.g., retroicor) (Behzadi et al., 2007). To further minimize the potential influence of motion-related artifacts, we also regressed from the BOLD time series of each ROI the 6 realignment parameters, their first-order temporal derivatives and their associated quadratic terms (24 regressors in total, cf. Bolt et al., 2017). Our goal was to isolate task-related functional coupling from mere co-activation effects corresponding to the beginning and end of a task event (i.e., two regions that are both activated at the beginning of a task event and de-activated at the end of a task, although they do not "communicate" with one another throughout the task event). Consequently, the initial and final scans within each 18 s task event were de-weighted by applying to the BOLD timeseries of each ROI a regressor, obtained by convolving a boxcar task design function with the hemodynamic response function, and its first temporal order derivative (cf. Braun et al., 2015; Vatansever et al., 2015; Westphal et al., 2017; Whitfield-Gabrieli and Nieto-Castanon, 2012). The residual BOLD time series were bandpass filtered (0.008 Hz $<$ f $<$ 0.09 Hz), linearly detrended and despiked (all three are default CONN denoising steps). Following these corrections (which did not include global signal regression), an inspection of each subject's histogram of voxel-to-voxel connectivity values across all scrutinized task conditions revealed a normal distribution, approximately centered around zero, which would suggest reduced contamination from physiological and motion-related confounds (cf. Whitfield-Gabrieli and Nieto-Castanon, 2012). We compared these histograms with those obtained after applying global signal regression instead of CompCor. As can be seen in Fig. S1, CompCor was more effective at removing physiological and motion-related confounds (i.e., the relevant histograms showed less biased distributions). We assume that this is because signal from the CSF and WM captures most noise-related variance and CompCor regresses out five components from each. In contrast, through global signal regression only one WM and one CSF component are regressed out, in addition to the global signal from gray matter, which, at least in this case, does not seem to make a substantial contribution to artifact removal.

1.1.7. fMRI data analysis

1.1.7.1. ROI time series. 229 nodes for 10 networks (i.e., default [DMN], frontoparietal [FPC], cingulo-opercular [CON], salience [SAL], dorsal attention [DAN], ventral attention [VAN], somatomotor [SM], subcortical [SUB], auditory [AUD] and visual [VIS]) were defined for each participant as spherical ROIs (radius 5 mm) centered on the coordinates of the regions reported in Power et al. (2011) and assigned network labels corresponding to the graph analyses from this earlier article. The ROIs were created in FSL (Smith et al., 2004), using its standard 2 mm isotropic space, with each ROI containing 81 voxels. These template space dimensions were selected because they yielded the most adequate spatial representation of the Power atlas. The 229 ROIs represent a subset of the 264 putative functional areas proposed by Power et al. (2011). The 229 ROIs were selected because, based on Power et al.'s analyses, they showed relatively unambiguous membership to one of the ten functional networks outlined above.

1.1.7.2. ROI-to-ROI connectivity analyses. For each patient and control participant, we used the CONN toolbox to compute pairwise bivariate correlations among all 229 ROIs during each of the ten task conditions (i.e., four time periods for the autobiographical memory task and one odd/even number judgment condition for each of the two scanning sessions). The patients' versus controls' neural profiles specific to each time period will be described elsewhere. The goal of the present report is to characterize the unique features that distinguish the functional architecture supporting episodic autobiographical memory from a non-episodic generic task (i.e., number judgment) architecture among severely depressed patients versus healthy controls. Consequently, to identify for each individual, at each of the two time points, the functional brain organization underlying mental travel to a specific past event, irrespective of its remoteness, we averaged the four correlation matrices corresponding to the four autobiographical memory periods under scrutiny (one week, one month, one year and ten years). Thus, for each of the two scrutinized tasks (i.e., autobiographical memory vs. number judgment), 360 TRs (720 s) went into the construction of the associated correlation matrices. For patients who generated fewer than the required 40 events (see Table 1), the same number of TRs were dropped from their number judgment condition in order to ensure that any differences in functional brain organization between conditions are not due to duration. For all analyses, the pairwise correlations among all the ROIs were expressed as Fisher's z-scores.

Consistent with existing practices aimed at maximizing interpretability of results in neural network studies of individual or group differences (e.g., sex or age, Betzel et al., 2014; Satterthwaite et al., 2015), we used both positive and negative z-scores to compute the indices of interest for all connectivity analyses. We reasoned that such an approach would be particularly well-justified in our present case since global signal regression, an artifact removal technique that yields negative connectivity values, whose interpretation is still controversial, was not part of our preprocessing pipeline (for further discussion on the validity of the negative correlations obtained with the CONN toolbox, see Whitfield-Gabrieli and Nieto-Castanon, 2012).

1.1.7.3. Whole-brain functional organization. For each participant, within each task condition (episodic memory-time 1, number judgment-time 1, episodic memory-time 2, number judgment-time 2), we estimated whole-brain functional organization by employing a Louvain community detection algorithm implemented in the Brain Connectivity Toolbox (BCT, Rubinov and Sporns, 2010). This algorithm partitions a network into non-overlapping groups of nodes with the goal of maximizing an objective modularity Q function (Rubinov and Sporns, 2011; Betzel and Bassett, 2017). For each ROI entered in an analysis, the algorithm identifies a community (i.e., group of other ROIs) with which it is affiliated during the scrutinized task condition. For signed networks, such as the ones investigated in our study, optimization of the Q function can be achieved by either placing equal weight on maximizing positive within-module connections and minimizing negative within-module connections or by putting a premium on maximizing positive connections, which have been argued to be of greater biological significance (Rubinov and Sporns, 2011). Although we verified that all the reported results emerge with either formula, for the sake of simplicity and because we agree with their argument regarding the greater importance of positive weights in determining node grouping into communities, we report here the results based on Rubinov and Sporns's modularity formula (cf. Chen et al., 2016). In this formula, the contribution of positive weights to Q is not affected by the presence of negative weights in the network, whereas the contribution of negative weights to Q decreases with an increase in positive weights. The adapted modularity function Q*, proposed by Rubinov and Sporns (2011) is written as

$$Q^{*} = \frac{1}{v^{+}} \sum_{ij} (w_{ij}^{+} - \gamma e_{ij}^{+}) \delta_{M_i M_j} - \frac{1}{v^{+} + v^{-}} \sum_{ij} (w_{ij}^{-} - \gamma e_{ij}^{-}) \delta_{M_i M_j}.$$

where $\delta_{MiMj} = 1$ if nodes i and j are in the same module and $\delta_{MiMj} = 0$ otherwise; v^{+} and v^{-} constitute the sum of all positive (w^{+}) and all negative (w^{-}) weights in the network, respectively; $w_{ij}^{\pm}$ represent the actual within-module positive or negative connection weights with $w^{\pm} \in (0,1]$; γ is a resolution parameter determining the size of the identified modules; $e_{ij}^{\pm}$ is the within-module connection strength expected by chance and defined, for each node-to-node (i,j) connection as $e_{ij}^{\pm} = \frac{s_i^{\pm} s_j^{\pm}}{v^{\pm}}$, with $s_i^{\pm}$ and $s_j^{\pm}$ being the sum of all positive or all negative connection weights of node i and j, respectively,

while $v^{\pm}$ is the sum of all positive or all negative connection weights in the network.

The value of the resolution parameter γ determines the size of the communities identified with a Louvain community detection algorithm and, as such, it may affect estimates of community structure. Because we did not have any specific hypotheses regarding community size, we followed extant practices in the literature and computed all the relevant network metrics for three values of the spatial resolution parameter centered around 1 (γ values of 1.00, 0.95 and 1.05, cf. Braun et al., 2015). All the steps described below for computing agreement matrices were implemented separately for each value of the γ resolution parameter.

It has been shown that the modularity function Q (in its various forms) may show extreme degeneracy, which means that the maximal modularity partition is "hidden" among a relatively large number of "near-perfect" modularity partitions, which are nonetheless structurally dissimilar from one another (Good, de Montjoye, & Clauset, 2010). In order to address the fact that the optimization landscape is characterized by the existence of this plateau of high modularity partitions, we followed existing practices in the literature (cf. Braun et al., 2015; Chen et al., 2016). Thus, the Louvain algorithm was initiated 100 times.

Following the 100 iterations of the community detection algorithm, run in each of the four task conditions (episodic memory at time 1, number judgment at time 1, episodic memory at time 2, number judgment at time 2) and for each of the three gamma values, we obtained, for each participant, twelve task-related matrices. Each of these matrices contained each node's assignment to a community across the 100 whole-brain partitions. Subsequently, we used the BCT to compute an agreement matrix for each participant in each of the four task conditions and for each value of the gamma parameter. Each entry in this matrix contains the number of times that a given ROI pair was assigned to the same community across the 100 iterations of the modularity algorithm in each task condition and for each value of the gamma parameter. Using the BCT, each participant's agreement matrix was rescaled, so that all matrix entries fell within the [0,1] interval. Hence, each entry in this rescaled matrix reflected the probability that two ROIs belonged to the same community.

Subsequently, based on the idea that core structural aspects of a network are stable across variations of the estimation parameters (cf. Betzel and Bassett, 2017), we averaged the three agreement matrices corresponding to the three gamma values in order to obtain a probabilistic representation of each participant's "true" community structure within each task context at each of the two timepoints. In the four resulting matrices, entries with higher values corresponded to those ROI pairs that were more likely to be assigned to the same community across the three gamma values in each task condition. In order to obtain a probabilistic representation of community structure across individuals as a function of task (the episodic memory versus the number judgment) and group membership (patients versus controls), the participant-specific agreement matrices were entered into a task PLS analysis (see below).

To confirm the validity of our results, we also ran all the reported analyses for each individual value of the spatial resolution parameter (i.e., 0.95, 1, 1.05). All the results described below were replicated. Hence, for the reasons outlined above (i.e., identification of the true, stable "core" of the autobiographical memory versus number judgment task architectures) and for the sake of concision, all the reported analyses used the agreement matrices averaged across the three values of the spatial resolution parameter herein scrutinized.

1.1.7.4. Brain-behavior analyses

1.1.7.4.1. Task-based partial least-squares correlation (task PLS). To identify features of the brain's functional architecture that distinguish between the two scrutinized task contexts (autobiographical memory versus the number judgment) as a function of assessment time (time 1/pre-ECT versus time 2/post-ECT) and group membership (patients versus controls), we employed PLS (Krishnan et al., 2011), a multivariate technique, powerful enough to be used with samples even smaller than ours (McIntosh and Lobaugh, 2004), which can identify in an unconstrained, data-driven manner, neural patterns (i.e., latent variables or LVs) related to different experimental conditions (task PLS). In PLS, data decomposition is performed in one step, hence eliminating the need for multiple comparison correction.

It has been argued that PLS can be regarded as a hybrid between completely hypothesis-driven (e.g., univariate general linear models [GLM]) and completely data-driven (e.g., independent components analysis [ICA]) approaches (Lin et al., 2003). Indeed, unlike ICA, the data decomposition is not performed across all possible dimensions, but it is restricted to the identified experimental conditions and/or groups. Nevertheless, PLS is also distinct from completely hypothesis-driven approaches, which test a single hypothesized contrast across conditions (i.e., univariate GLM). Instead, PLS identifies the most robust contrasts in the data, provides an estimate of how much of the covariance in the data each component accounts for and indicates the brain pattern that tracks with the identified contrasts. Consequently, within the framework of PLS, if a hypothesized contrast emerges as significant, it means that it represents a robust way of distinguishing among the brain patterns associated with different experimental conditions and/or groups.

PLS was run on graph theoretical estimates of ROI-to-ROI coupling, rather than being run directly on Pearson's *r* correlations in ROI time series. We opted to do so because the former reflects pairwise ROI-to-ROI functional association strength (i.e., likelihood of two ROIs being assigned to the same community), which takes into consideration individual-specific whole-brain functional organization. Specifically, the aforementioned graph theoretical measures provide a means for placing a specific ROI-to-ROI correlation coefficient in the context of the remaining ROI-to-ROI correlation coefficients, thereby ascribing it functional significance with respect to the "breakdown" of the whole brain into non-overlapping communities of ROIs for each individual participant. This "contextualization" is particularly important in light of recent evidence of the unique information contained in individual-defined whole brain functional architecture (Gordon et al., 2017). Consequently, we reasoned that consistent cross-patient changes in functional brain architecture, induced by ECT, would be more adequately characterized if we applied PLS to indices of ROI-to-ROI functional association strength, which took into consideration individual-specific functional brain organization. We should though point out that the PLS-identified neural patterns reported below also emerge, albeit somewhat more weakly, when PLS is run on Pearson's r correlations in ROI time series. The fact that the PLS-identified patterns are weaker when PLS is run on coefficients of functional coupling which do not take into consideration individual-specific functional architecture is not surprising to us given aforementioned evidence of the unique information contained in individual-specific brain architecture (Gordon et al., 2017).

PLS was implemented using a series of Matlab scripts, which are available for download at https://www.rotman-baycrest.on.ca/index.php?section=345. We conducted a sole task-PLS analysis in which we entered patients' and controls' autobiographical memory and number judgment data at both time points. In this analysis, one matrix corresponded to the brain data, whereas the second matrix corresponded to the task design data. The brain matrix contained each participant's concatenated episodic memory and number judgment task agreement matrices, at time 1 and time 2, respectively. The patients and the controls were modeled as separate groups in all PLS analyses. Thus, the design matrix contained a number of dummy coded variables corresponding to each experimental condition within each group (e.g. the patients' autobiographical memory condition at time 1). Based on these matrices, PLS extracted pairs of LVs, specifically, one LV based on the brain matrix and one LV based on the design matrix, with the constraint that each pair of LVs shares the maximum amount of covariance possible. By introducing the patients' and controls' data from both time

points in the same PLS analysis, we were able to test whether the patterns identified by PLS as explaining the most variance in our data are compatible with our hypothesis that ECT corrects the patients' brain organization patterns in the autobiographical memory, specifically (i.e., renders the patients' brain organization patterns more similar to those of controls in this condition). By introducing the two groups in the same analysis, we were also able to test whether the patterns identified by PLS as explaining the most variance in our data support the hypothesis of a reliable brain organization profile linked to trait depression (i.e., a neural profile that distinguishes patients from controls at both time points).

In all the reported analyses, the significance of each LV was determined using a permutation test with 5000 permutations (in the permutation test, the rows of the brain data are randomly reordered, Krishnan et al., 2011). In the case of our present analyses, PLS assigned to each ROI-to-ROI pair a weight, which reflected the respective pair's contribution to a specific LV. Here, a higher value positive weight would characterize those ROI-to-ROI pairs whose assignment to the same community would constitute a more salient feature of an identified functional brain organization pattern. Complementarily, a negative weight higher in absolute value would characterize those ROI-to-ROI pairs whose assignment to different communities would constitute a more salient feature of an identified functional brain organization pattern. The reliability of each pair's contribution to a particular LV was tested by submitting all weights to a bootstrap estimation (1000 bootstraps) of the standard errors (SEs, Efron, 1981) (the bootstrap samples were obtained by sampling with replacement from the participants, Krishnan et al., 2011). We opted to use 5000 permutations and 1000 bootstrap samples in order to increase the stability of the reported results, since these parameters are ten times greater than the standard ones (i.e., 500 permutations/100 bootstrap samples), recommended by McIntosh and Lobaugh (2004) for use in PLS analyses of neuroimaging data. A bootstrap ratio (BSR) (weight/SE) of at least 4 in absolute value (approximate associated *p*-value of .0001) was used as a threshold for determining those ROI-to-ROI pairs that made a significant contribution to the identified LVs. The BSR is analogous to a z-score, so an absolute value > 2 is thought to make a reliable contribution to the LV (Krishnan et al., 2011), although for neuroimaging data BSR absolute values > 3 tend to be used (McIntosh and Lobaugh, 2004). Potential axis rotations (i.e., changes in the order of the extracted LVs) and reflections (i.e., changes in the sign of the saliences), which may occur during resampling with either permutations or bootstrapping, were corrected with a Procrustes rotation, which defines a transformation through which the resampled singular value decomposition outcome (i.e., the identified LVs) is rotated to match most closely the original singular value decomposition outcome (Milan & Whittaker, 1995).

Because decisions regarding thresholding (see BSR above) are somewhat arbitrary, we present both the raw and thresholded brain patterns. To facilitate network-level interpretations, we also include graphical renditions of the identified LVs in which the contributions of the individual connections are aggregated at the level of the entire functional network (see Figs. 1b, d and 2b, d).

1.1.7.4.2. Task PLS LV scores: pre- to post-ECT change scores. The PLS analysis described below identified two brain organization patterns, one that distinguished patients from controls across both task contexts and time points (i.e., the trait depression LV) and a second LV which was specific to the autobiographical memory context and susceptible to “normalization” through ECT. To estimate similarity between the trait depression versus the ECT-correctable neural profile and each patient's functional brain organization within each task context at each time point, we used the weights associated with each ROI-to-ROI pair in each of the two brain LVs to compute separate LV1 versus LV2 scores as weighted sums across all ROI-to-ROI pairs. An individual's higher scores on LV1 or LV2 indicated greater similarity between his or her functional brain organization and the trait depression (LV1) or the ECT-corrected (LV2) neural profile.

At each of the two time points, a total LV 1 score in the autobiographical memory condition was created by averaging the corresponding LV 1 scores at both time points. This score was relevant to our hypothesis regarding the link between the trait depression neural profile and affective persistence (i.e., ruminative tendencies), which we expected to emerge in the autobiographical memory condition. Complementarily, keeping with its task-related pattern (see Results below and Fig. 2e), a total LV 2 score was created by subtracting the LV 2 score in the number judgment condition from the LV 2 score in the autobiographical memory condition at each time point. A change score in LV2 was operationalized as the residual resulting from regression of the post-ECT LV 2 total score onto the corresponding pre-ECT total score. For LV2, we focused on all task conditions because at the whole brain level LV2 reflected the degree of differentiation between the autobiographical memory and the number judgment task.

1.2. Results

1.2.1. Functional task architecture pre- vs. post-ECT[2]

1.2.1.1. LV #1: Patients vs. controls. The first significant LV, revealed by the task PLS ($p = .0002$), accounted for 33.47% of the variance in the data and differentiated the functional brain architecture typical of patients versus controls across both time points and task contexts (see Fig. 1). Relative to controls, patients showed greater fragmentation within FPC (i.e., the FPC ROIs were more likely to be assigned to different communities among patients relative to controls), as well as greater segregation between FPC and the remaining two control networks (SAL, most strongly, and, to a lesser degree, CON) (see Fig. 1b, d). They also demonstrated greater integration (i.e., assignment to the same community) of the SM ROIs with those from networks involved in control initiation (SAL, FPC) and, to a lesser degree, with those implicated in external attention (DAN, VAN) (see Fig. 1b,d). At the level of individual ROI-to-ROI connections, the patients were typified by greater integration of the FPC and midline DMN (aMPFC, PCC) ROIs (eight connections) (see Fig. 1a,c).

1.2.1.2. LV #2: ECT-induced functional brain reorganization. The second significant LV ($p = .0002$) explained 16.61% of the variance in the data and differentiated the functional brain architecture that supported performance on the autobiographical memory (for patients only post-ECT) from that which supported performance on the number judgment task (see Fig. 2). Compared to the number judgment task, the functional brain organization typical of the episodic memory task was most reliably characterized by greater segregation between the system implicated in top-down control (FPC) and the two external attention networks (VAN, DAN) (see Fig. 2d), stronger fragmentation within FPC, greater separation between the two control initiation systems (FPC, SAL), as well as between VIS and AUD (see Fig. 2b,d). At the level of individual ROI-to-ROI connections, the autobiographical memory task was distinguished by reliably (BSR > 4) greater integration of MTL ROIs with both VIS (nine connections) and FPC ROIs (four connections), as well as of midline DMN (PCC, aMPFC) with FPC ROIs (six connections) (see Fig. 2a, c).

[2] The task-PLS revealed also a third LV ($p = .0002$), which accounted for 13.73% of the variance in the data and differentiated the ROI-to-ROI connections recruited by patients post-ECT during the autobiographical memory task from the connections recruited by controls during the autobiographical memory task at both time points. Nonetheless, in control analyses in which we used ART in the CONN toolbox to eliminate outlier scans (i.e., relative scan-to-scan global signal z-value threshold of 3 and a 0.5 mm relative movement threshold), the two LVs, described in the main text were reproduced well, whereas the third LV was not. Given its lower reliability, we opted to not include this LV in the main report.

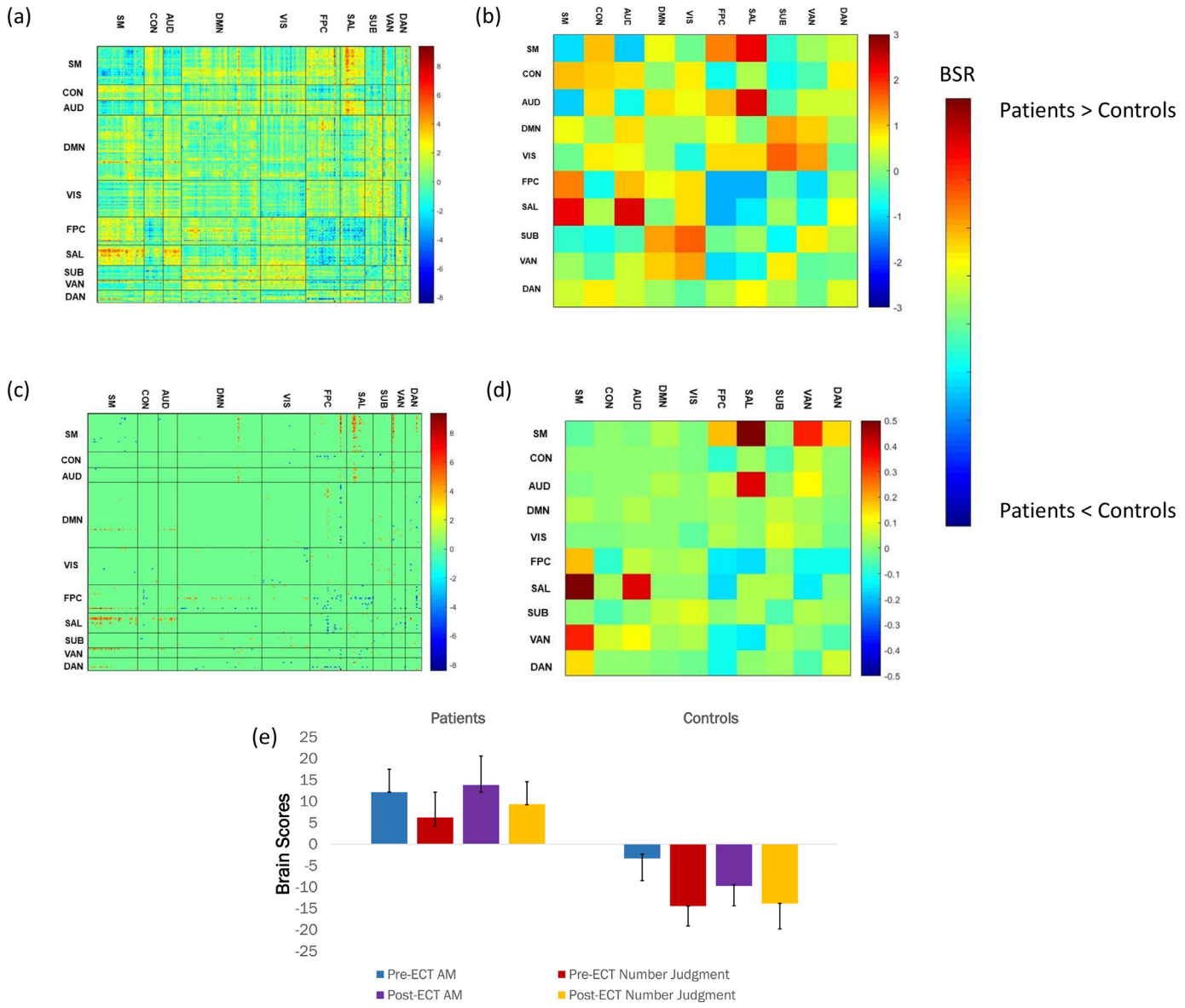

Fig. 1. Functional organization patterns that differentiate patients from healthy comparison participants both before and after ECT. Panel (a) shows all the ROI-to-ROI connections that are stronger (warm colors) versus weaker (cool colors) in patients relative to controls. Panel (b) presents a network-level summary of the results presented in panel (a). Panel (c) shows the ROI-to-ROI connections that are reliably (absolute value BSR ≥ 4) stronger (warm colors) versus weaker (cool colors) in patients relative to controls. Panel (d) presents a network-level summary of the results presented in panel (c). In panels (c) and (d) connections that did not meet the aforementioned BSR threshold were set to zero. Panel (e) shows the average of the mean-centered brain scores from the task PLS analysis for each condition (error bars are the 95% confidence intervals [CI] from the bootstrap procedure). Non-overlapping CIs indicate statistically significant differences between conditions. Please note that the brain scores do not have meaningful units since they are computed as the weighted sum of all ROI-to-ROI connections entered in the PLS analysis.

1.2.2. Control analyses

Mann-Whitney tests unveiled significant differences in age ($p = .043$) and session 1-to-session 2 delay ($p = .007$) between patients and controls. Of these two, only age differences were relevant to LV1, whereas both age and session delay could potentially impact greater expression of LV2-associated patterns at time 2. However, Mann-Whitney tests revealed that residual LV1 scores, controlled for age, were still significantly higher among patients relative to controls across both tasks and time points (all $ps < .0001$). Similarly, Spearman's correlation analysis revealed no statistically significant association between either age or session 1 to session 2 delay and LV2 change score (i.e., time 2 expression controlling for time 1 expression), both $ps > .77$.

1.2.3. Functional task architecture and cognitive performance

The analyses described below were based on data from all 15 patients (see *"Task PLS LV scores: Pre- to post-ECT change scores"* section above on how LV1 and LV2 scores were computed for each patient). Although employing the data from the five patients who did not understand or comply with the task demands could have impacted the reliability of the functional brain organization patterns identified with PLS, we reasoned that these patients' LV1 and LV2 scores should nonetheless be related to our cognitive variables of interest in a way similar to the one observed in the core sample of 10 patients (i.e., addition of the five patients could have added noise to our brain-behavior analyses, but should not have reversed the overall patterns). To confirm our assumption, we ran all the relevant analyses for the core patient sample only. These results are presented in the brackets next to the effects obtained with the full sample of 15 patients. Sex was introduced

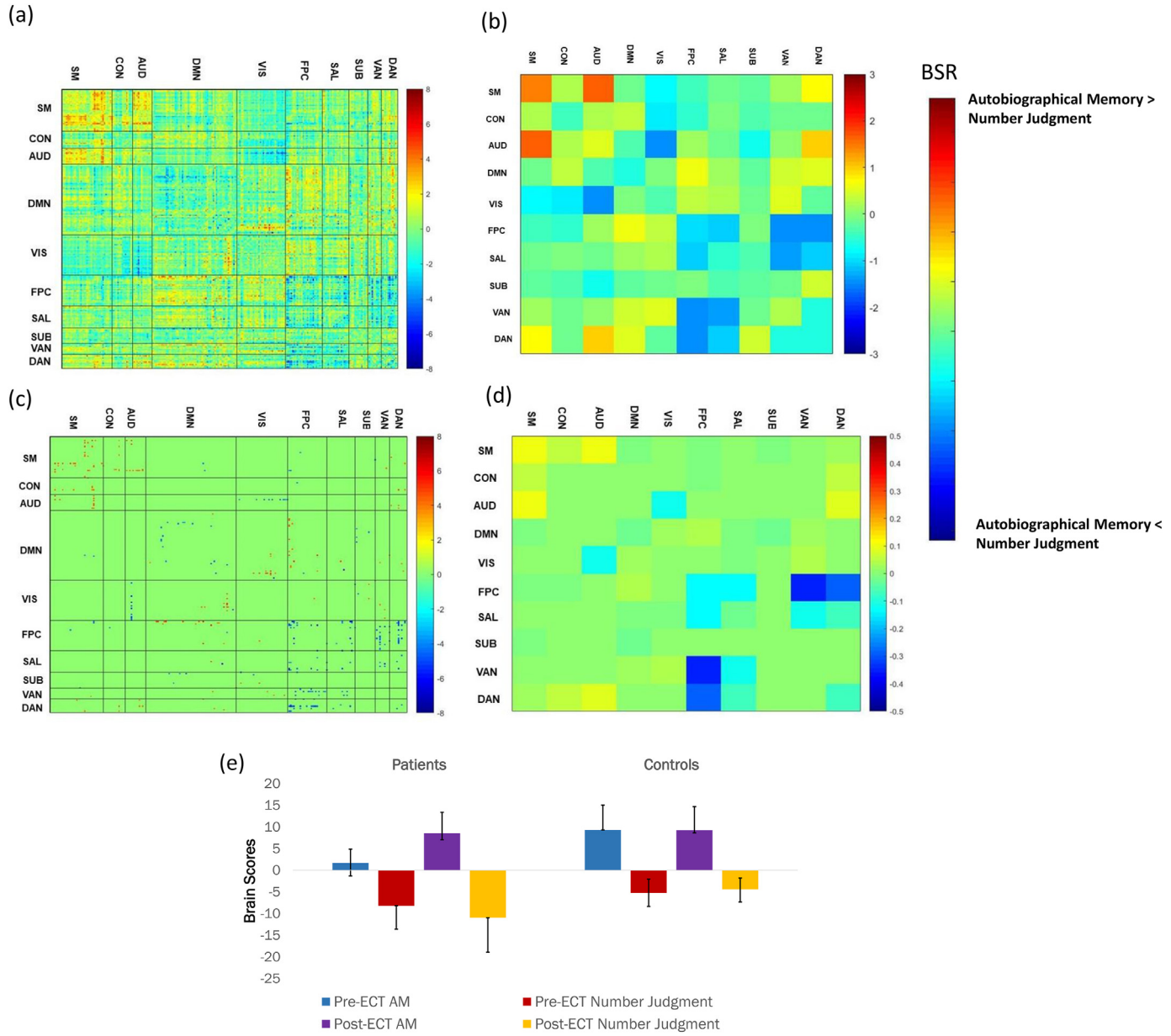

Fig. 2. Functional organization patterns that differentiate the autobiographical memory from the number judgment task. Panel (a) shows all the ROI-to-ROI connections that are stronger (warm colors) versus weaker (cool colors) in the autobiographical memory relative to the number judgment task. Panel (b) presents a network-level summary of the results presented in panel (a). Panel (c) shows the ROI-to-ROI connections that are reliably (absolute value BSR ≥ 4) stronger (warm colors) versus weaker (cool colors) in the autobiographical memory relative to the number judgment task. Panel (d) presents a network-level summary of the results presented in panel (c). In panels (c) and (d) connections that did not meet the aforementioned BSR threshold were set to zero. Panel (e) shows the average of the mean-centered brain scores from the task PLS analysis for each condition (error bars are the 95% confidence intervals [CI] from the bootstrap procedure). Non-overlapping CIs indicate statistically significant differences between conditions. Please note that the brain scores do not have meaningful units since they are computed as the weighted sum of all ROI-to-ROI connections entered in the PLS analysis.

as a covariate in all analyses to confirm that all reported effects apply to both male and female patients. Below, greater expression of LV 1 versus LV 2 implies greater similarity to the trait depression versus the ECT-corrected functional brain architecture.

1.2.3.1. Pre- to post-ECT changes in functional task architecture and neuropsychological test performance. Greater post-ECT expression of LV 2 was associated with greater post-ECT improvements in visuospatial learning, Spearman's *rho* = .58, $p = .023$ (see Fig. 3a; [10 patients: *rho* of .39, $p = .26$]).

1.2.3.2. Depression-relevant functional task architecture and autobiographical memory persistence. Secondly, we tested the hypothesis that the psychopathological trait-like features, captured by LV 1, reflect dispositional patterns of cognitive-affective persistence, a likely building block of the ruminative thinking profile that typifies depression. To this end, we investigated whether, in the autobiographical memory condition, at both time points (this LV was not affected by ECT), LV 1 would be more strongly expressed by those individuals who recall events that are thought of or talked about more frequently (i.e., events that are more persistent in the rememberer's mind). We found that this was indeed the case, Spearman's *rho* = .57, $p = .027$ (see Fig. 3b; [10 patients: *rho* of .36, $p = .31$]).

In sum, up to this point, we presented suggestive evidence on the

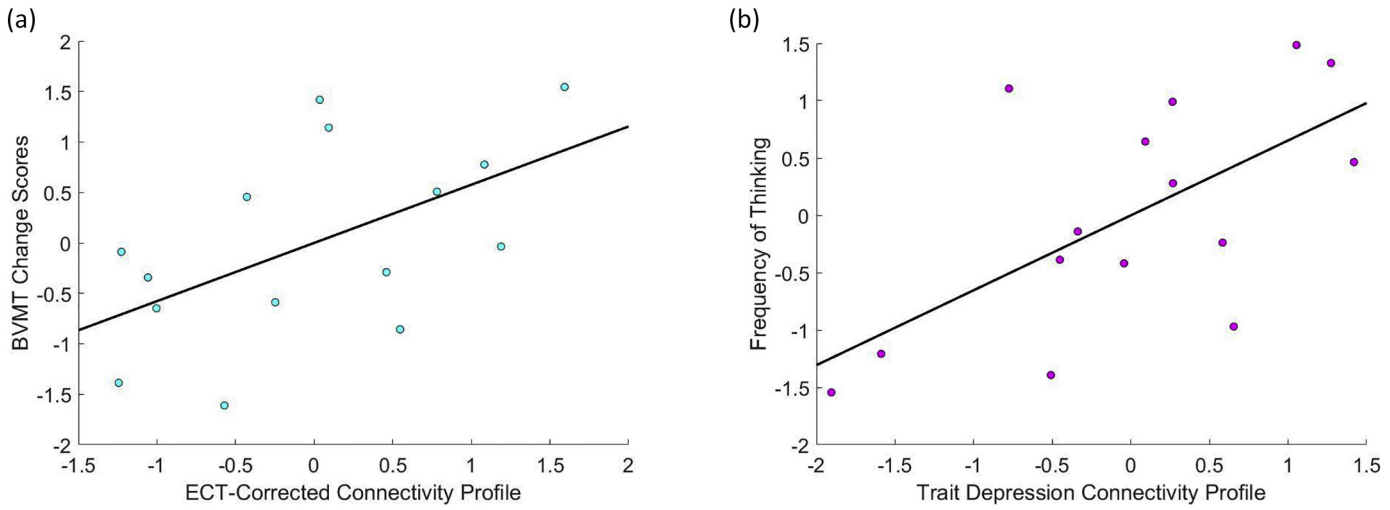

Fig. 3. The relationship between the two whole-brain connectivity LVs, identified through task PLS and neuropsychological test performance (panel a), autobiographical memory characteristics (panel b). All variables have been standardized.

distinguishable brain organization patterns linked to trait depression versus those "corrected" by ECT (and related to post-ECT cognitive improvement). Next, we sought to test our hypothesis that the observed ECT-normalized neural pattern reflects neurocognitive mechanisms, which, in the healthy population, may counteract the experience of depressogenic tendencies (see Part 2 below). Moreover, we attempted to characterize the extent to which such mechanisms, as expressed in contexts relevant to visuospatial learning (i.e., online maintenance of visuospatial representations, perceptual relational processing) are susceptible to genetic versus environmental contributions. This question was pursued in order to establish the suitability of the aforementioned neurocognitive mechanisms as risk and/or potential intervention targets for increasing resilience among at-risk individuals (see Part 3 below).

2. Part 2: HCP sample 1

2.1. Method

2.1.1. Participants

The sample included 333 individuals who were part of the Human Connectome Project (HCP) and whose data had been released as part of the HCP 1200 subjects data package in March 2017. This sample size represented the largest number of participants from the HCP 1200 subjects data release who were unrelated to one another, who did not overlap with the twin pairs, confirmed through genetic testing (see HCP Sample 2 below), and who had available data on all the behavioral and fMRI assessments of interest.

The majority of participants ($N = 300$) were right-handed. The sample included 169 younger men (51 between 22 and 25, 69 between 26 and 30, and 49 between 31 and 36 years of age) and 164 younger women (50 between 22 and 25, 49 between 26 and 30, and 65 between 31 and 36 years of age). Although age is presented here in the range format, as advocated by the HCP team (see Van Essen et al., 2012 for the rationale behind this age reporting strategy in HCP data releases), all our brain-behavior analyses used participants' actual age in years, as available in the HCP restricted data release.

All participants were screened for a history of neurological and psychiatric conditions and use of psychotropic drugs, as well as for physical conditions or bodily implants that may render their participation unsafe. Diagnosis with a mental health disorder and structural abnormalities, as revealed by the MRI structural scans, were also exclusion criteria. Participants provided informed consent in accordance with the HCP research ethics board.

2.1.2. Depression-relevant cognitive-affective profiles

Scores on the scales and tasks described below were available in the HCP 1200 subjects data release. The depression/anxiety scales and the delay discounting task were completed on Day 1 of the participants' HCP schedule, while the list sorting task and the questionnaires on current affective experience were completed on Day 2.

2.1.2.1. Affective persistence. The decay in the subjective value of delayed rewards, which was our proxy for affective persistence, was assessed with a discounting task that identifies "indifference points" at which an individual is equally likely to choose a smaller reward (e.g., $50) sooner versus a larger reward later ($200 in one year). In this task, the delays are fixed, but the value of the immediate reward is varied in order to identify as swiftly as possible an individual's indifference point (see also Estle et al., 2006; Green et al., 2007; Myerson et al., 2001). The task uses the area-under-the curve (AUC) as a performance measure with separate indices for a large ($40,000) versus a small ($200) monetary amount. Because we did not have any distinct hypotheses regarding the two values and the two demonstrated identical relationships with the neural variables of interest, we present the analyses based on the average value of the AUC for the small and large reward, where higher values indicate greater subjective value associated with the delayed reward.

2.1.2.2. Learning. As a measure of the participants' ability to encode and mentally manipulate information, we used the NIH Toolbox List Sorting Test. We reasoned that this task was the closest analogue in the HCP task battery to the visuospatial learning task, which yielded significant effects in the ECT sample. In the List Sorting task, participants are presented with pictures of foods or animals, each accompanied by a sound clip and written text that identify the respective item. List length varies from two to seven items. In the 1-List condition, participants have to arrange either food items or animals in size order from smallest to largest. In the 2-List condition, they are presented with food items as well as animals and are required to report the food items first in size order, followed by the animals in size order. The outcome measure is the number of correctly recalled items (i.e., lists). For an item to be considered correct, all its constituents need to be reported in the correct size order.

2.1.2.3. Subclinical depression and anxiety. To assess relatively stable subclinical variations in depression and anxiety, we used participants' scores on the DSM-oriented depression and anxiety scales. Both sets of scores were derived from participants' responses to relevant items on

the Achenbach Adult Self-Report (ASR) instrument for ages 18–59 (Achenbach, 2009). The ASR contains a total of 123 statements relevant to psychological functioning and requires participants to rate on a 3-point scale (0 *not true*, 1 somewhat or sometimes true, 2 *very true or often true*) how well each item described them over the previous six months. The DSM-oriented depression scale includes items such as "I cry a lot.", "I am unhappy, sad, or depressed", "I deliberately try to hurt or kill myself", "I feel tired without good reason.", "There is very little that I enjoy.". The DSM-oriented anxiety scale includes items such as " I worry about my future", "I am too fearful or anxious.".

2.1.2.4. Current negative emotion experience. Participants completed the NIH Toolbox Negative Affect Survey, which assesses separately current levels of experienced sadness (e.g., "I felt sad.","I felt like a failure."), anger (e.g., "I felt angry.", "I felt bitter about things."), and fear (e.g., "I felt frightened.', "I had a racing or pounding heart."), respectively. The measure requires participants to rate on a 5-point scale (1 *never* to 5 *always*) how often they experienced the relevant emotion within the past seven days.

2.1.3. fMRI tasks

We included all the fMRI tasks that are part of the Human Connectome Project with the exception of the emotion processing task. In our opinion, this task would have added novel information only if we could analyze separately its two component conditions (face versus shape processing), since their shared variance is likely redundant with the one assessed by the static relational processing task, whose results are easier to interpret. Given that the duration of each component condition in the emotion task is approximately 126 s, we reasoned that their inclusion would affect adversely the reliability of our reported functional organization patterns.

2.1.3.1. Working memory. Participants completed two runs of an n-back task, which included as targets four categories of stimuli: faces, places, tools and body parts. Each run encompassed 8 task blocks (27.5 s each) and 4 fixation blocks (15 s each). The 8 task blocks corresponded to two working memory tasks (2-back versus 0-back), with each comprising all four stimulus categories, presented in separate blocks. In the 2-back working memory task, participants had to respond 'target' whenever the current stimulus was the same as the one presented two trials before. In the 0-back working memory task, a condition that is most similar to traditional delayed match-to-sample tests, a stimulus was presented at the beginning of each block and the participants had to respond "target" whenever the respective stimulus was encountered during the block. Each block began with the 2.5 s presentation of a cue indicating task type and, for the 0-back task only, target stimulus, followed by 10 trials of 2.5 s each (2 s stimulus presentation and 500 ms interstimulus interval) for a total block duration of 27.5 s. Each block contained 2 targets and 2–3 non-target lures (e.g., repeated items in the wrong n-back position, either 1-back or 3-back) to ensure that participants are actively drawing on their memory resources to complete the task (for further discussion, see Barch et al., 2013).

2.1.3.2. Static relational processing. This task was adapted from the one developed by Christoff and colleagues (Smith, Keramatian, & Christoff, 2007). The task features six different shapes filled with one of six different textures. In the relational processing condition, participants see two pairs of objects, one at the top and the second at the bottom of the screen. They are asked to identify first the dimension on which the top pair differs (shape or texture) and then decide whether the bottom pair of objects differs along the same dimension. In the item-based matching condition, participants see a pair of objects at the top of the screen and one object at the bottom of the screen. Participants are asked to determine whether the bottom object matches either of the two top objects on the dimension ("shape" or 'texture") identified by a word presented in the middle of the screen. Each of the two task runs comprises three 16 s long relational, matching and fixation blocks, respectively. Each relational block contains four trials. On each trial, stimuli are presented for 3500 ms with a 500 ms interstimulus interval. Each matching block comprises five trials. On each trial, stimuli are presented for 2800 ms, followed by a 400 ms interstimulus interval.

2.1.3.3. Dynamic relational processing (social cognition). Participants completed two runs of a task, adapted from Castelli et al. (2000) and Wheatley et al. (2007), in which they were presented with short videos (20 s) of objects (squares, circles, triangles), either interacting in a purposeful manner or just moving randomly across the screen. After each video, the participants had to decide among three alternative answers: (1) *Social Interaction*: the video portrayed a social interaction (i.e., an interaction in which the shapes appear to take into account each other's thoughts and emotions); (2) *Not Sure* (whether the video depicted a social interaction or just random movement); (3) *No Interaction*: the video showed shapes moving randomly across the screen. Each of the two task runs has 5 video blocks of 23 s each (2 Mental and 3 Random in one run, 3 Mental and 2 Random in the other run) and 5 fixation blocks (15 s each).

2.1.3.4. Financial incentive processing. Participants completed two runs of a task, adapted from Delgado et al. (2000), in which they were required to guess the number on a mystery card (represented by a "?") in order to win or lose money. They were told that potential card numbers ranged from 1 to 9 and were asked to indicate if they thought the mystery card number was more or < 5 by pressing one of two buttons on the response box. Feedback is the number on the card (generated by the program, after the participants made their guess, as a function of whether the trial was a reward, loss or neutral trial) and either: 1) a green up arrow with "$1" for reward trials, 2) a red down arrow next to −$0.50 for loss trials; or 3) the number 5 and a gray double headed arrow for neutral trials. The "?" was presented for up to 1.5 s (if the participant responded before 1.5 s, a fixation cross was displayed for the remaining time), followed by the feedback for 1 s. There was a 1 s interstimulus interval with a "+" presented on the screen. The task was presented in blocks of 8 trials that were either mostly reward (6 reward trials pseudo-randomly interleaved with either 1 neutral and 1 loss trial, 2 neutral trials, or 2 loss trials) or mostly loss (6 loss trials interleaved with either 1 neutral and 1 reward trial, 2 neutral trials, or 2 reward trials). In each of the two runs, there were 2 mostly reward and 2 mostly loss blocks (28 s each), interleaved with 4 fixation blocks (15 s each).

2.1.3.5. Language/mathematical processing. Participants completed two runs of a task, adapted from Binder et al. (2011), in which aural presentation of brief stories alternates with aural presentation of math problems. On each run, participants are presented with four story and four math blocks, which are matched in duration (each is approximately 30 s long). On the story blocks, participants are presented with short adaptations of Aesop's fables (5–9 sentences), which involve animal and human characters interacting in easily understandable social situations. Subsequently, participants are required to answer a two-alternative forced choice question, which tests their understanding of the story topic. On the math blocks, participants are asked to solve addition and subtraction problems. Each trial features an arithmetic operation (e.g., "fourteen plus eighteen"), followed by "equals", then two alternatives (e.g., "thirty-two or twenty-eight"). The math task is adapted on an individual basis, so that a similar level of difficulty is maintained across subjects.

2.1.3.6. Motor function. This task was adapted from the one developed by Buckner and colleagues (Buckner et al., 2011; Yeo et al., 2011). In response to visual cues, participants are required to tap their left or right fingers, squeeze their left or right toes, or move their tongue. Each

block, corresponding to a movement type, lasts 12 s (10 movements) and is preceded by a 3 s cue. In each of the two task runs, there are two tongue, four finger (two left, two right) and four toe (two left, two right) movement blocks, respectively, as well as three 15 s fixation blocks.

2.1.4. fMRI data acquisition

Images were acquired with a customized Siemens 3 T "Connectome Skyra" scanner housed at Washington University in St. Louis (32-channel coil). Pulse and respiration were measured during scanning. T1-weighted anatomical scans were acquired with a 3D MP-RAGE sequence (TR = 2400 ms, TE = 2.14 ms, FOV = 224 mm, 320 × 320 matrix, 256 slices of 0.7 mm isotropic voxels). The high-resolution structural scan preceded the acquisition of functional scans.

Functional images were acquired with a multiband EPI sequence (TR = 720 ms, TE = 33.1 ms, flip angle = 52°, FOV = 208 mm, 104 × 90 matrix, 72 slices of 2 × 2 mm in-plane resolution, 2 mm thick, no gap). For each task, two runs of equal duration were obtained, one collected with a L-R, and the other, with a R-L, EPI phase coding sequence. The length of one run (in minutes) was as follows: 5:01 (working memory), 2:56 (relational processing), 3:27 (social cognition), - 3:12 (incentive processing), 3:57 (language/math) and 3:34 (motor).

Individual L-R and R-L scans exhibit distinct regions of complete signal loss, but it has been verified that the preprocessed datasets are anatomically well-aligned with one another, even in areas of complete signal loss (cf. Smith et al., 2013). Because it is only the dropout that differs between the two scan types, it has been recommended that connectivity analyses based on HCP data aggregate the respective metrics from the L-R and R-L scans (cf. Smith et al., 2013). Consequently, in the present report, we concatenated the L-R and R-L runs for each task.

2.1.5. fMRI data Preprocessing

The present report used the preprocessed task data from the HCP 1200 subjects data release. These data have all been preprocessed with version 3 of the HCP spatial and temporal pipelines (Smith et al., 2013; for specification of preprocessing pipeline version, see http://www.humanconnectome.org/data). Additionally, we used the CONN toolbox to implement the same denoising steps applied to the data from the ECT sample. Following all these corrections (which did not include global signal regression), an inspection of each subject's histogram of voxel-to-voxel connectivity values for each scrutinized task condition revealed a normal distribution, approximately centered around zero, which would suggest reduced contamination from physiological and motion-related confounds (cf. Whitfield-Gabrieli and Nieto-Castanon, 2012). Nonetheless, in supplementary analyses, accompanying all the brain-behavior tests, we confirmed that all the reported effects were not driven by individual differences in motion, as they remained unchanged after controlling for the average relative (i.e., volume-to-volume) displacement per participant, a widely used motion metric (Power et al., 2012, 2015; Satterthwaite et al., 2013).

2.1.6. fMRI data analysis

2.1.6.1. ROI time series. We followed the same procedure we used with our ECT sample.

2.1.6.2. ROI-to-ROI connectivity analyses. Pairwise coupling among the 229 ROIs was estimated in CONN, separately for each task condition.

2.1.6.3. Whole-brain functional organization. We followed the same procedure we used with our ECT sample. To ensure similar durations for all scrutinized task conditions, we estimated whole-brain functional organization independently in the zero-back and two-back condition of the working memory task, as well as in the story and math condition of the language task. Importantly, this breakdown of the working memory and language task, respectively, also respected the distinguishable cognitive requirements of their component conditions (zero-back versus two-back; story versus math). Thus, the task-relevant connectivity matrices were based on durations ranging from 192 s (i.e., static relational processing) to approximately 230 s (motor function). After conducting our network-level analyses, we were left with eight agreement matrices per participant, one matrix for each task condition (zero-back, two-back, static relational, dynamic relational, story, math, gambling and motor). Entries with higher values corresponded to those ROI pairs that were most likely to be assigned to the same community across the three values of the spatial resolution parameter and 100 iterations of the community detection algorithm, performed within each task and for each value of the spatial resolution parameter.

2.1.6.4. Brain-behavior analyses

2.1.6.4.1. PLS: Depression-relevant functional task architecture. To estimate similarity between the trait depression versus the ECT-correctable neural profile and each HCP participant's functional brain organization during each scrutinized task condition, we used the corresponding connection weights obtained from the task PLS analysis, conducted on the clinical sample, to calculate "LV scores". These LV scores (i.e., two per task context per participant) were computed as the weighted sum across all ROI-to-ROI pairs and were employed in all the analyses described next. When computing these LV scores, we included all connections and not only those with a BSR > 4 in absolute value in the ECT sample because we reasoned that this approach would yield the most accurate representation of the two LVs. Specifically, reliability thresholds are somewhat arbitrarily determined and it was the two whole-brain connectivity patterns, to which all the connections contributed, that were found to be significantly different from noise in the permutation testing conducted in the ECT sample.

2.1.6.4.2. Canonical correlation analysis (CCA). To identify the relationship between the depression-relevant cognitive and neural indices, we used canonical correlation analysis (CCA, Hotelling, 1936). CCA is a multivariate technique, which seeks maximal correlations between two sets of variables by creating linear combinations (i.e., canonical variates) from the variables within each set. Recently, CCA has been successfully used to investigate the relationship between brain connectivity patterns and cognitive-behavioral variables, broadly defined (e.g., age, education, cognition, affect, drug and alcohol use) in large datasets (see Smith et al., 2015; Tsvetanov et al., 2016; Vatansever et al., 2017). CCA was implemented using the canoncorr function in Matlab. The significance of each canonical variate pair was tested by using a permutation test (i.e., shuffling of the brain data across subjects) with 100,000 permutations (cf. Smith et al., 2015).

To describe the relationship between the behavioral or brain variables and their corresponding variates (i.e., latent factors), we include canonical loadings (cf. Hair Jr. et al., 2009), which reflect the raw correlation between a brain or behavioral variable and its corresponding variate (see also Tsvetanov et al., 2016). In order to obtain reliable estimates of canonical loadings, CCA requires a sample size at least ten times the number of variables in the analysis (Hair et al., 1998). Our sample size exceeded this criterion for all analyses. Although there are no established procedures for ascribing statistical significance to canonical loadings, the latter are homologous to factor loadings, which is why it has been recommended that they be subjected to similar interpretive criteria (Hair et al., 1998).2.1.6.4.2.1. Univariate and multivariate outliers

Univariate and multivariate outliers can adversely impact data normality and, thus, have the potential to bias the results of canonical correlation analyses (Sherry & Henson, 2005). Because all the effects remained unchanged if univariate (z-scores lower than −3.29 or > 3.29) and multivariate (Mahalanobis distance-based) outliers had been eliminated, we opted to report the results based on the full sample.

2.2. Results

To test our hypothesis that some of the therapeutic effects of ECT are due to its boosting the expression of a naturally occurring neural profile relevant to visuospatial learning, which counteracts the experience of depressogenic tendencies in the general population, we conducted a canonical correlation analysis (CCA). In this CCA, we entered affective persistence, list sorting, subclinical depression, subclinical anxiety, as well as currently experienced anger, fear and sadness as part of the behavioral set. Scores on the trait depression- and ECT-relevant neural LVs, assessed in each of the eight scrutinized task contexts (zero-back, two-back, static relational processing, dynamic relational processing, financial incentive processing, semantic processing, math and motor function) were part of the brain set (sixteen brain variables in total). This analysis revealed only one significant CCA mode ($r = 0.44$, $p = 4 \times 10^{-5}$, see Fig. 4a for loadings of each connectivity and cognitive variable on its respective canonical variate, as well as Fig. 4b for the relationship between the brain and behavioral canonical variates). Specifically, individuals with a depressogenic cognitive profile (higher affective persistence, poorer learning), worse current affective experience and greater mood-related (anxiety, depression) symptomatology showed greater expression of the trait depression LV and reduced expression of the ECT-linked LV across both working memory (zero-back, two-back) and relational processing (static, dynamic) task conditions, as well as, unexpectedly, in the math condition. To account for potential demographic and motion-related confounds, we regressed out from all the behavioral variables, entered in CCA #1 above, handedness, gender, age, years of education, as well as the average volume-to-volume displacement across all the scrutinized task contexts. A second CCA, conducted on these residual behavioral scores and the same brain scores entered in CCA #1, revealed a sole significant canonical mode ($r = .42$, $p = .001$) and almost identical canonical loadings for both the behavioral and brain variables as those identified in CCA #1 (see Fig. S2a for loadings of each connectivity and cognitive variable on its respective canonical variate, as well as Fig. S2b for the relationship between the brain and behavioral canonical variates).

2.2.1. Control analysis

To verify that the aforementioned CCA results involving affective persistence are not merely an artifact of reduced responsiveness to reward, we capitalized on the established finding that the subjective value of larger delayed rewards decays more slowly relative to the value of smaller delayed rewards (Myerson et al., 2001). This effect was replicated in the present sample when comparing the subjective value of the delayed \$200 vs. 40 K, $t(332) = -21.32$, $p = .0001$.

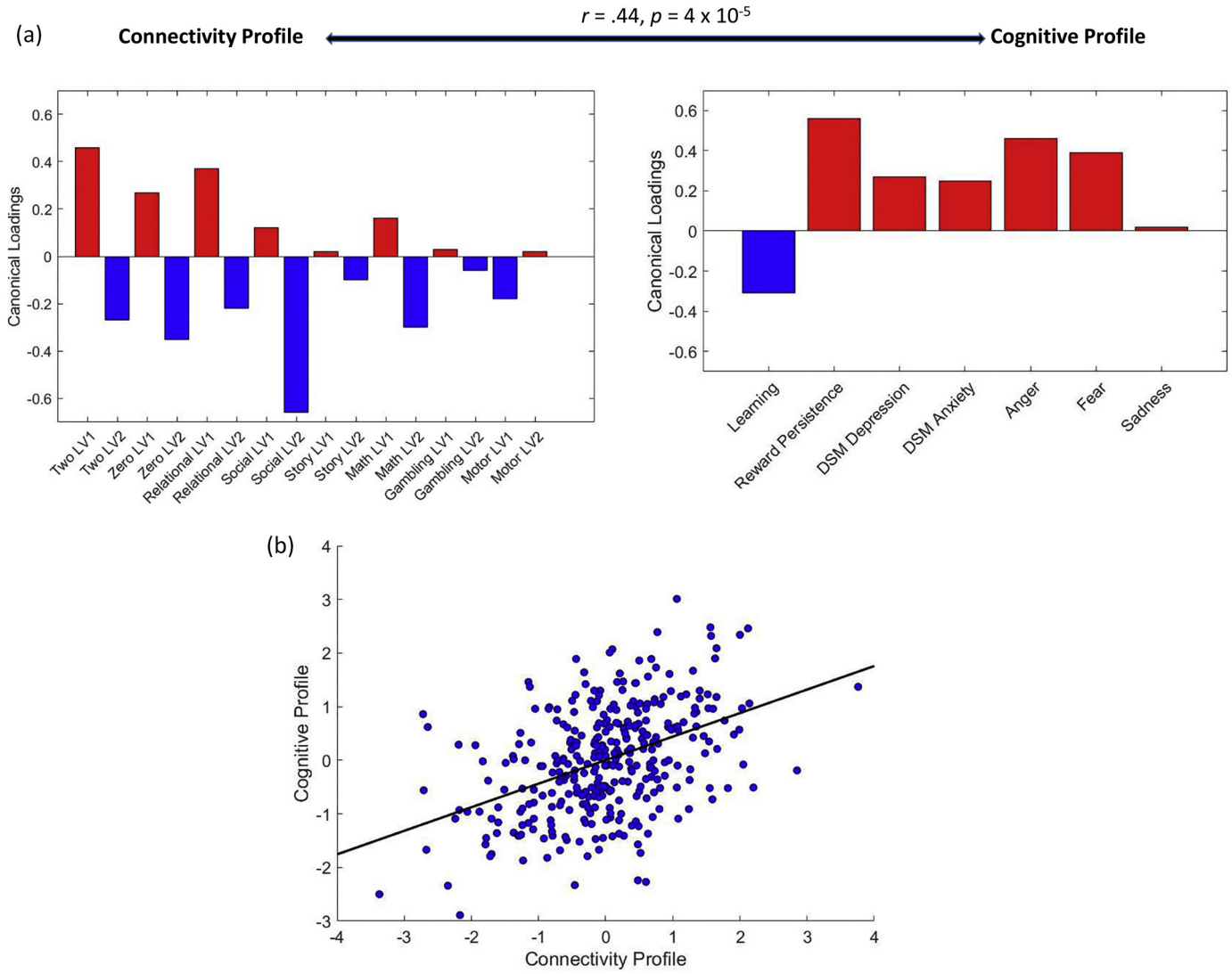

Fig. 4. The loadings of the brain and behavioral variables from CCA #1 on their corresponding canonical variates (panel [a]) and the scatter plots describing the linear association between the brain and the behavioral canonical variates (panel [b]).

Subsequently, we created a residual score by regressing out from the reward persistence score, described above, the difference in the subjective value of the delayed $200 vs. 40 K, which indicated the extent to which participants showed a differentiated response to reward based on its value. The CCA results, described above remained unchanged when using this residual reward persistence score. This suggests that our findings are unlikely to be due to atypical responses to reward, but instead they are more likely to reflect perpetuation of motivational value across time, as we proposed.

3. Part 3: HCP sample 2

3.1. Method

3.1.1. Participants

This sample comprised the largest number of twin pairs from the HCP 1200 subjects data release, whose zygosity had been confirmed through genetic testing, who had available fMRI data on all the variables of interest and who allowed us to keep a ratio of 1:1 for DZ versus MZ pairs, which is recommended as optimal for providing equal power to detect genetic versus environmental influences (Verhulst, 2017). The sample included 64 DZ (58 males: 24 between 22 and 25, 26 between 26 and 30, and 8 between 31 and 36 years of age; 70 females: 42 between 26 and 30, and 28 between 31 and 36 years of age) and 64 MZ (58 males: 12 between 22 and 25, 32 between 26 and 30, and 14 between 31 and 36 years of age; 70 females: 40 between 26 and 30, and 30 between 31 and 36 years of age) pairs. An independent samples *t*-test confirmed that there were no statistically significant differences in age between the DZ and the MZ pairs ($p > .39$). The majority of Sample 2 participants ($N = 237$) were right-handed and self-identified as being White ($N = 228$). This sample was subject to the same exclusion criteria as the HCP Sample 1.

3.1.2. fMRI tasks

Participants completed the same tasks as the HCP Sample 1.

3.1.3. fMRI data acquisition

All the image acquisition parameters were identical to the ones described for the HCP Sample 1.

3.1.4. fMRI data Preprocessing

We followed the same preprocessing steps described for the HCP Sample 1.

3.1.5. fMRI data analysis

To increase reliability (i.e., estimate network structure based on more TRs) and in line with their conceptual similarity with respect to the underlying cognitive processes assessed, we averaged the ROI-to-ROI correlation matrices corresponding to zero-back and two-back conditions (average *r* between these two matrices across all participants of 0.36 ± 0.06), as well as those corresponding to static and dynamic relational processing (average *r of* 0.23 ± 0.05). With respect to the network-level analyses and projection of the two depression-linked whole-brain connectivity patterns in each of the two scrutinized task contexts (online maintenance versus relational processing), we followed the same steps as the ones outlined for the HCP Sample 1.

3.1.6. Genetic analyses

To characterize genetic versus environmental influences on the expression of the two depression-relevant neural connectivity patterns, we ran two series of analyses, one using an *ACE* (A = additive genetic effects; C = shared environmental effects; E = unique environmental effects) and the second, an ADE (A = additive genetic effects; D = dominant genetic effects; E = unique environmental effects), structural equation model (Neale and Cardon, 1992), implemented in Mplus 8.0 (Muthén & Muthén, 1998–2017) and applied to the fMRI data from the HCP Sample 2. Such analyses rest on the fact that the MZ twins share 100% of their genes, whereas the DZ twins share ~50% of their genes. Hence assuming full genetic determination via additive effects, the MZ twin correlation on a specific trait should be 1, whereas the DZ correlation should be 0.50. Full genetic determination via dominant effects would yield MZ twin correlations of 1 on a specific trait and DZ twin correlations of 0.25. DZ twin correlations greater than half of the MZ twin correlations on a given trait are indicative of shared environmental effects, whereas MZ twin correlations lower than 1 are said to reflect non-shared environmental influences on the trait under comparison.

In twins reared together, as is the case of our present sample, dominant genetic and shared environmental effects may not be disentangled, which is why ACE and ADE models need to be estimated separately. The ACE/ADE model was set up as a two-group (MZ vs. DZ) analysis. A, C, D and E are modeled as latent factors that affect the trait under scrutiny. The twin correlation between the corresponding C factors is set to 1 when both types of twin pairs are reared together (i.e., the shared environment is equivalent), as it is the case in the present study. The twin correlation between the corresponding A factors is set to 1 for the MZ pairs because they share 100% of their genes and to 0.50 for the DZ pairs who share ~50% of their genes. Following the same rationale, the twin correlation between the corresponding D factors is set to 1 for the MZ pairs and to 0.25 for the DZ pairs. The correlations between the corresponding E factors are set to zero because by definition these environmental effects are individual-specific, reflecting unique environmental effects and measurement error.

In addition to the chi-square statistic, which assesses the discrepancy between the observed and the fitted covariance matrices (i.e., values closer to zero mean better fit), but is very sensitive to sample size, we report two widely used measures of fit that take into consideration both sample size and model complexity. One is the root-mean-square error of approximation (RMSEA) statistic, an absolute fit index that quantifies how well the covariances predicted by the model match the observed covariances. The second is the Tucker–Lewis index (TLI), a non-normed (i.e., can exceed 1.0, but is still reported as 1.0 in these cases) incremental fit index that quantifies how well the model fits compared with a null model (in our case, a model with only variances but no covariances among the measures). Based on guidelines from Hu and Bentler (1998), we used RMSEA < .06 and TLI > .95 as markers of good fit.

3.2. Results

Our ACE/ADE model analyses, corroborated by an inspection of the raw correlation matrices, suggested that the two depression-relevant LVs show distinct patterns of heritability in the online maintenance versus the perceptual relational processing condition (see Fig. 5). Specifically, in the former context, both LVs demonstrated substantial additive genetic effects, whereas in the latter condition it was only the ECT-linked LV that showed evidence of significant heritability (i.e., dominant genetic effects). These results raise the possibility that the two depression-relevant neural patterns, identified in the ECT sample, are most closely linked to contexts that require integration of externally oriented processing (i.e., vigilance to the environment) with internal cognition (i.e., online maintenance of relevant mental representations).

4. Discussion

Although ECT is a widely used and effective treatment for refractory depression, the precise neural substrates underlying its therapeutic effects remain to be fully elucidated (but see Dukart et al., 2014). To address this issue, the present study tested the hypothesis that some of the beneficial effects of ECT are due to its stimulating the expression of a naturally occurring neurocognitive profile relevant to visuospatial learning, which, in the healthy population, may help counteract the

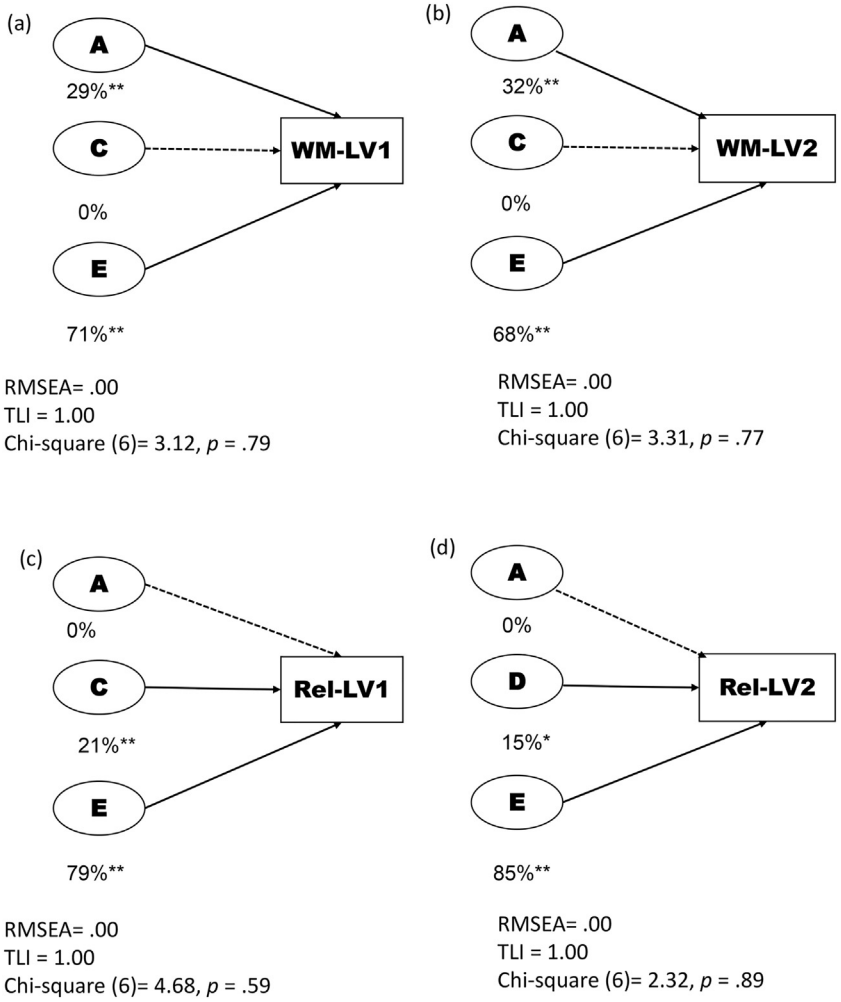

Fig. 5. The ACE/ADE models associated with the expression of the LV 1- and LV 2-related brain organization patterns during working memory (panels a and b) and relational processing (panels c and d). The percentages next to the ACEs/ADEs represent the percentage of variance explained by additive genetic (A), dominant genetic (D), common environmental (C) and unique environmental (E) factors. Dashed lines represent non-significant effects ($p > .05$). *$p < .05$. **$p < .0001$.

experience of depressogenic tendencies. To establish its suitability as a risk marker and/or intervention target, we quantified its susceptibility to genetic versus environmental factors. Thus, by pinpointing neural pathways in depression and their response to clinical intervention, the present research contributed to existing efforts to establish viable targets for early detection and treatment of depressive symptomatology.

One important finding of our study was the identification of a specific whole brain functional organization pattern, which was found to be susceptible to correction through ECT and whose stronger expression among healthy individuals was associated with fewer affective markers of global psychopathology and fewer depression-relevant cognitive deficits. In the clinical sample, the aforementioned brain organization pattern was specific to an episodic autobiographical memory task, in which patients were asked to visualize past personal events. As expected, given the role of visuospatial processing in autobiographical recall in general (Daselaar et al., 2008; Greenberg et al., 2005; Vannucci et al., 2016), and, in our task, in particular, post-ECT "normalization" of the neural profile specific to the autobiographical memory context was related to improvements in attending to, specifically, learning, visuospatial information, a cognitive function which is significantly impaired in major depression, but which is reportedly responsive to ECT (Mohn and Rund, 2016; Semkovska and McLoughlin, 2010). Although there was no autobiographical memory task in the HCP sample, we were able to assess the relevance of the ECT-correctable pattern for performance of cognitive tasks that draw upon the related functions of visuospatial working memory and perceptual relational processing, which are also affected in depression (Baune et al., 2014; Korgaonkar et al., 2013; Lee et al., 2005; Rose and Ebmeier, 2006; Schneider et al., 2012; Söderlund et al., 2014).

The brain pattern susceptible to "correction" through ECT was typified by a host of neural markers linked to mental scene construction in the service of past, present or future-oriented episodic simulation (i.e., greater integration of the MTL ROIs with both the VIS and FPC ROIs [Fig. 2a,c], but increased fragmentation within the FPC [Fig. 2b, d]) among healthy individuals (Andrews-Hanna et al., 2014b; Andrews-Hanna et al., 2014a; Corbetta and Shulman, 2002; Seeley et al., 2007; Sheldon et al., 2016; Spreng et al., 2010, 2014; Sridharan et al., 2008; Westphal et al., 2017). Additionally, it was also characterized by greater segregation between top-down control (FPC) and attentional (VAN, DAN) systems (Fig. 2d), implying diminished goal-directed external processing (Spreng et al., 2010, 2014), as well as greater separation between the two control initiation systems (FPC, SAL), which may suggest more efficient implementation of "supervisory" processes (Braun et al., 2015; Sporns and Betzel, 2016). Although the precise mechanisms of ECT are unknown, our results suggest that ECT may "normalize" access to a cognitive mode that fosters episodic simulation through the goal-directed integration of perceptual and mental representations. However, its acceleration of neurogenesis and systems level functional reorganization disrupts access to previously acquired memories (Farzan et al., 2017; Frankland and Josselyn, 2016) and, in

general, is known to impair recollection for information acquired pre-ECT (i.e., retrograde amnesia, cf. Sackheim, 2014; Semkovska and McLoughlin, 2014; Söderlund, Percy, & Levine, 2012). Accordingly, in our study, the patients' expression of the ECT brain pattern was related to performance on the BVMT-R, a task assessing memory for visual information acquired post-ECT.

Complementarily, we identified a whole brain functional organization pattern linked to trait depression and rumination in the clinical sample that was associated with greater incidence of depressogenic tendencies, both cognitive and affective, among healthy adults. This pattern was most clearly expressed as stronger functional coupling between internal cognition (DMN) and internally driven control (FPC) ROIs (see Fig. 1a, c), greater integration of the SM with control networks (SAL, FPC), as well as greater segregation within and between the latter (Fig. 1b, d) (Andrews-Hanna et al., 2010; Spreng et al., 2010; Sridharan et al., 2008) These findings are compatible with existing views on depression which highlight the potential for raw somato-affective states to contaminate and, thus, impair cognitive control processes (Dolcos et al., 2011; McTeague et al., 2017; McTeague et al., 2016; Opel et al., 2017; Ramirez-Mahaluf et al., 2017). These results also dovetail a substantial body of evidence on the role of self-focused thinking in guiding cognitive-behavioral control processes, as well as on the tight intertwining of self-referential and raw somatic states in the affective persistence (i.e., ruminative) processes associated with major depression (Burkhouse et al., 2017; Cooney et al., 2010; Davey et al., 2017; Davey et al., 2016; Hamilton et al., 2015; Jones et al., 2017; Rayner et al., 2016).

Finally, expanding the existing repertoire of structural and brain activity markers associated with intergenerational transmission of depression (Foland-Ross et al., 2016; Foland-Ross et al., 2015; Gotlib et al., 2014; Opel et al., 2017), we have provided evidence on the heritability of the two functional brain organization patterns relevant to depression, as identified in the ECT sample. Specifically, we have shown that they demonstrate substantial susceptibility to genetic influences in a cognitive context that hinges on visuospatial processing that extends *beyond* the here-and-now, but much less so in a context that requires perceptual processing *in* the here-and-now. Given that the expression of the two LVs during the two aforementioned contexts, working memory versus perceptual relational processing, made similarly strong contributions to depression-relevant cognition and affect in HCP sample 1 (see Fig. 4a), we find it unlikely that their differential heritability patterns, as observed in HCP sample 2, would merely reflect measurement error (i.e., such measurement error would have adversely impacted the contribution of these two LVs in HCP sample 1). While we cannot completely rule it out, we think it is more likely that the context-specific heritability of the two LVs speak to their unique relevance to tasks that require temporally extended processing of visuospatial information and, thus, integration of internal cognition with externally oriented perceptual processing. The fact that LV2 shows both substantial heritability and susceptibility to change, as revealed by the ECT intervention and genetic analyses (i.e., the E component, which we argued above is unlikely to only reflect measurement error) renders it a viable marker for vulnerability to global psychopathology (as per the HCP sample 1 results), as well as a locus for assessing success of interventions targeting cognitive deficits linked to mood-related pathology. Although contexts that require visuospatial processing extended beyond the here-and-now may be of particular interest, results from the HCP sample 1 suggest that LV2 may be a particularly sensitive tracker of improvements in the social deficits associated with depression (see Fig. 4a; Lee et al., 2005; Schneider et al., 2012). Further investigations are also needed on the nature of the genetic effects to which the two LVs appear to be susceptible. For example, given the relative context specificity of the behavioral effects linked to the two LVs (see Fig. 4a), the question arises as to how genes may impact responses to specific environmental learning circumstances in a way that leads to the emergence of the neural configurations observed for LV1 and 2, respectively.

Due to pragmatic considerations related to the availability of such a vulnerable population, we were able to test only a relatively small sample of severely depressed patients who underwent ECT (similar sample sizes for patients and controls have though been used by others as well, e.g., Dukart et al., 2014; Ristow et al., 2018). While we acknowledge the limitations of our present sample size, our core ECT sample was relatively homogenous, as it only comprised patients with a diagnosis of severe major depressive disorder, thereby rendering it unlikely that the observed functional brain organization patterns were contaminated by co-existing conditions. We employed powerful statistical tools (i.e., PLS) that are well-suited for use with sample sizes even smaller than ours (cf. McIntosh and Lobaugh, 2004) and both of the reported patterns of functional brain organization, which we set out to characterize, emerged as highly significantly different from noise (as per the permutation testing used to assess the statistical significance of the PLS-identified LVs in the ECT sample). Importantly, as outlined above, our identified pattern of whole brain functional organization linked to trait depression, the only one of the two herein characterized that has precedent in the literature, shares significant similarities with previously documented neural profiles of depression, thereby strengthening our confidence in our present results. Additionally, the fact that both of the LVs identified in the clinical sample showed the predicted robust associations with cognition and affect in HCP Sample 1 further testifies to their conceptual validity.

With regards to the ECT-linked pattern of brain organization, this is unlikely to merely reflect the influence of time as it emerged in the patient group following a therapeutic induction of seizures, with no corresponding change in the control group who was tested after a similar passage of time. Furthermore, it was context-specific and meaningfully associated with cognitive variables that did not show significant group-level changes from Time 1 to Time 2 (see Table 1). On the topic of sample size, we should mention that, although the size of our present twin sample is similar to that used in other brain-genetics investigations (e.g., Yang et al., 2016), future studies using larger twin samples and multiple assessments of connectivity (cf. Ge et al., 2017) may be needed to confirm our present findings.

Finally, future research may benefit from applying network-based analyses such as those described here to characterize the neural correlates of ECT-induced improvements in mood. Indeed, in our clinical sample, we found statistically significant reductions in BDI scores post-ECT, which were though unrelated to the expression of our two identified brain LVs. As we have already mentioned, our focus was on the mnemonic deficits that are associated with depression and susceptible to correction through ECT, which is what our fMRI tasks were designed to assess. We expected though that the neural organization patterns linked to post-ECT mnemonic amelioration would also be associated with post-ECT mood improvement. Nonetheless, our two identified brain LVs predicted affective functioning only in the HCP sample. This may speak to the superiority of the affective assessment tools used by the HCP (compared to the BDI), as well as to the fact that the much larger HCP sample afforded the identification of subtler brain-behavior relationships. Patient studies using explicitly affective tasks may be needed to characterize the changes in neural organization patterns specifically associated with ECT-induced corrections in mood. That being said, we would like to underscore that our two identified brain LVs do hold promise with respect to their clinical utility. First, they predicted both affective and cognitive problems in a healthy sample, testifying to their sensitivity to varying degrees of psychopathology in the general population. Second, the brain pattern susceptible to correction through ECT and related to improvements in visuospatial memory reflected normalization of functional network interactions relevant to autobiographical memory retrieval. As such, this brain pattern is likely relevant to the successful cognitive restructuring of past and future personal event representations, a key component in therapeutic interventions such as cognitive-behavioral therapy, as well as in self-

initiated attempts to repair mood.

In summary, the present study provided suggestive evidence that some of the therapeutic effects of ECT are due to its ability to "normalize" the expression of a neural profile relevant to visuospatial learning and personal event (re)construction, which shows some heritability, but which can nonetheless be also activated via relevant environmental learning experiences. As such, our research is directly relevant to future interventions aimed at increasing resilience among at-risk individuals by targeting intrinsic mechanisms which may help counteract the cognitive and affective deficits associated with depression, specifically, and global psychopathology, more broadly.

Supplementary data to this article can be found online at https://doi.org/10.1016/j.nicl.2019.101816.

Acknowledgments

Part of the data was provided by the Human Connectome Project, WU-Minn Consortium (Principal Investigators: David Van Essen and Kamil Ugurbil; 1U54MH091657) funded by the 16 NIH Institutes and Centers that support the NIH Blueprint for Neuroscience Research; and by the McDonnell Center for Systems Neuroscience at Washington University. This work was supported by the Canadian Institutes of Health Research MOP-62963 to B.L.

References

Achenbach, T.M., 2009. The Achenbach System of Empirically Based Assessment (ASEBA): development, findings, theory and applications. University of Vermont Research Center for Children, Youth and Families, Burlington, VT.

Andrews-Hanna, J.R., Reidler, J.S., Sepulcre, J., Poulin, R., Buckner, R.L., 2010. Functional–anatomic fractionation of the brain's default network. Neuron 65, 550–562.

Andrews-Hanna, J.R., Saxe, R., Yarkoni, T., 2014a. Contributions of episodic retrieval and mentalizing to autobiographical thought: evidence from functional neuroimaging, resting state connectivity, and fMRI meta-analyses. Neuroimage 91, 324–335.

Andrews-Hanna, J.R., Smallwood, J., Spreng, R.N., 2014b. The default network and self-generated thought: Component processes, dynamic control, and clinical relevance. Ann. N. Y. Acad. Sci. 1316, 29–52.

Barch, D.M., Burgess, G.C., Harms, M.P., Petersen, S.E., Schlaggar, B.L., Corbetta, M., Glasser, M.F., Curtiss, S., Dixit, S., Feldt, C., Nolan, D., Bryant, E., Hartley, T., Footer, O., Bjork, J.M., Poldrack, R., Smith, S., Johansen-Berg, H., Snyder, A.Z., Van Essen, D.C., for the WU-Minn HCP Consortium, 2013. Function in the human connectome: task-fMRI and individual differences in behavior. NeuroImage 80, 169–189.

Baune, B.T., Fuhr, M., Air, T., Hering, C., 2014. Neuropsychological functioning in adolescents and young adults with major depressive disorder—a review. Psychiatry Res. 218, 261–271.

Behzadi, Y., Restom, K., Liau, J., Liu, T.T., 2007. A component based noise correction method (CompCor) for BOLD and perfusion based fMRI. Neuroimage 37, 90–101.

Benedict, R., 1997. Brief Visuospatial Memory Test—Revised Professional Manual. Psychological Assessment Resources, Inc, Odessa, FL.

Benedict, R.H.B., Schretlen, D., Groninger, L., Brandt, J., 1998. Hopkins verbal learning test—revised: normative data and analysis of inter-form and test–retest reliability. Clin. Neuropsychol. 12, 43–55.

Betzel, R.F., Bassett, D.S., 2017. Multi-scale brain networks. NeuroImage 160, 73–83.

Betzel, R.F., Byrge, L., He, Y., Goñi, J., Zuo, X., Sporns, O., 2014. Changes in structuraland functional connectivity among resting-state networks across the human lifespan. Neuroimage 102, 345–357.

Binder, J.R., Gross, W.L., Allendorfer, J.B., Bonilha, L., Chapin, J., Edwards, J.C., Grabowski, T.J., Langfitt, J.T., Loring, D.W., Lowe, M.J., Koenig, K., Morgan, P.S., Ojemann, J.G., Rorden, C., Szaflarski, J.P., Tivarus, M.E., Weaver, K.E., 2011. Mapping anterior temporal lobe language areas with fMRI: a multicenter normative study. Neuroimage 54, 1465–1475.

Bolt, T., Nomi, J.S., Rubinov, M., Uddin, L.Q., 2017. Correspondence between evoked and intrinsic functional brain network configurations. Hum. Brain Mapp. 38, 1992–2007.

Braun, U., Schäfer, A., Walter, H., Erk, S., Romanczuk-Seiferth, N., Haddad, L., ... Bassett, D.S., 2015. Dynamic reconfiguration of frontal brain networks during executive cognition in humans. Proc. Natl. Acad. Sci. U. S. A. 112, 11678–11683.

Buckner, R.L., Krienen, F.M., Castellanos, A., Diaz, J.C., Yeo, B.T.T., 2011. The organization of the human cerebellum estimated by intrinsic functional connectivity. J. Neurophysiol. 106, 2322–2345.

Burkhouse, K.L., Jacobs, R.H., Peters, A.T., Ajilore, O., Watkins, E.R., Langenecker, S.A., 2017. Neural correlates of rumination in adolescents with remitted major depressive disorder and healthy controls. Cognit. Affect. Behav. Neurosci. 17, 394–405.

Castelli, F., Happe, F., Frith, U., Frith, C., 2000. Movement and mind: a functional imaging study of perception and interpretation of complex intentional movement patterns. NeuroImage 12, 314–325.

Chen, T., Cai, W., Ryali, S., Supekar, K., Menon, V., 2016. Distinct global brain dynamics and spatiotemporal organization of the salience network. PLoS Biol. 14, 21.

Cooney, R.E., Joormann, J., Eugène, F., Dennis, E.L., Gotlib, I.H., 2010. Neural correlates of rumination in depression. Cognit. Affect. Behav. Neurosci. 10, 470–478.

Corbetta, M., Shulman, G.L., 2002. Control of goal-directed and stimulus-driven attention in the brain. Nat. Rev. Neurosci. 3, 201–215.

Daselaar, S.M., Rice, H.J., Greenberg, D.L., Cabeza, R., LaBar, K.S., Rubin, D.C., 2008. The spatiotemporal dynamics of autobiographical memory: neural correlates of recall, emotional intensity, and reliving. Cereb. Cortex 18, 217–229.

Davey, C.G., Pujol, J., Harrison, B.J., 2016. Mapping the self in the brain's default mode network. NeuroImage 132, 390–397.

Davey, C.G., Breakspear, M., Pujol, J., Harrison, B.J., 2017. A brain model of disturbed self-appraisal in depression. Am. J. Psychiatry 174, 895–903.

Delgado, M.R., Nystrom, L.E., Fissell, C., Noll, D.C., Fiez, J.A., 2000. Tracking the hemodynamic responses to reward and punishment in the striatum. J. Neurophysiol. 84, 3072–3077.

Dolcos, F., Iordan, A.D., Dolcos, S., 2011. Neural correlates of emotion–cognition interactions: a review of evidence from brain imaging investigations. J. Cogn. Psychol. 23, 669–694.

Dukart, J., Regen, F., Kherif, F., Colla, M., Bajbouj, M., Heuser, I., ... Draganski, B., 2014. Electroconvulsive therapy-induced brain plasticity determines therapeutic outcome in mood disorders. Proc. Natl. Acad. Sci. U. S. A. 111, 1156–1161.

Efron, B., 1981. Nonparametric estimates of standard error: the jackknife, the bootstrap, and other methods. Biometrika 68, 589–599.

Estle, S.J., Green, L., Myerson, J., Holt, D.D., 2006. Differential effects of amount on temporal and probability discounting of gains and losses. Mem. Cogn. 34, 914–928.

Farzan, F., Atluri, S., Mei, Y., Moreno, S., Levinson, A.J., Blumberger, D.M., Daskalakis, Z.J., 2017. Brain temporal complexity in explaining the therapeutic and cognitive effects of seizure therapy. Brain J. Neurol. 140, 1011–1025.

First, M.B., Spitzer, R.L., Williams, J.B.W., Gibbon, M., 1995. Structured Clinical Interview for DSMIV-Patient Edition (SCID-P). American Psychiatric Press, Washington, DC.

Foland-Ross, L., Gilbert, B.L., Joormann, J., Gotlib, I.H., 2015. Neural markers of familial risk for depression: an investigation of cortical thickness abnormalities in healthy adolescent daughters of mothers with recurrent depression. J. Abnorm. Psychol. 124, 476–485.

Foland-Ross, L., Behzadian, N., LeMoult, J., Gotlib, I.H., 2016. Concordant patterns of brain structure in mothers with recurrent depression and their never-depressed daughters. Dev. Neurosci. 38, 115–123.

Frankland, P.W., Josselyn, S.A., 2016. Hippocampal neurogenesis and memory clearance. Neuropsychopharmacology 41, 382–383.

Ge, T., Holmes, A.J., Buckner, R.L., Smoller, J.W., Sabuncu, M.R., 2017. Heritability analysis with repeat measurements and its application to resting-state functional connectivity. Proc. Natl. Acad. Sci. U. S. A. 114, 5521–5526.

Good, B.H., de Montjoye, Y.A., Clauset, A., 2010. Performance of modularity maximization in practical contexts. Phys. Rev. E. Stat. Nonlin. Soft. Matter. Phys. 81, 046106.

Gordon, E.M., Laumann, T.O., Gilmore, A.W., Newbold, D.J., Greene, D.J., Berg, J.J., ... Dosenbach, N.U.F., 2017. Precision functional mapping of individual human brains. Neuron 95 (4), 791–807.

Gotlib, I.H., Joormann, J., Foland-Ross, L., 2014. Understanding familial risk for depression: a 25-year perspective. Perspect. Psychol. Sci. 9, 94–108.

Gratton, C., Laumann, T.O., Nielsen, A.N., Greene, D.J., Gordon, E.M., Gilmore, A.W., ... Petersen, S.E., 2018. Functional brain networks are dominated by stable group and individual factors, not cognitive or daily variation. Neuron 98, 439–452.

Green, L., Myerson, J., Shah, A.K., Estle, S.J., Holt, D.D., 2007. Do adjusting-amount and adjusting-delay procedures produce equivalent estimates of subjective value in pigeons? J. Exp. Anal. Behav. 87, 337–347.

Greenberg, D.L., Eacott, M.J., Brechin, D., Rubin, D.C., 2005. Visual memory loss and autobiographical amnesia: a case study. Neuropsychologia 43, 1493–1502.

Hair Jr., J.F., Black, W.C., Babin, B.J., Anderson, R.E., 2009. Multivariate Data Analysis, Seventh ed. Prentice Hall, Upper Saddle River, pp. 761.

Hair, J.F., Tatham, R.L., Anderson, R.E., Black, W., 1998. Multivariate data analysis, Fifth ed. Prentice-Hall, London.

Hamilton, J.P., Farmer, M., Fogelman, P., Gotlib, I.H., 2015. Depressive rumination, the default-mode network, and the dark matter of clinical neuroscience. Biol. Psychiatry 78, 224–230.

Hotelling, H., 1936. Relations between two sets of variables. Biometrika 28, 321–377.

Hu, L., Bentler, P.M., 1998. Fit indices in covariance structure modeling: sensitivity to underparameterized model misspecification. Psychol. Methods 3, 424–453.

Husain, M.M., Rush, A.J., Fink, M., Knapp, R., Petrides, G., Rummans, T., ... Kellner, C.H., 2004. Speed of response and remission in major depressive disorder with acute electroconvulsive therapy (ECT): a consortium for research in ECT (CORE) report. J. Clin. Psychiatry 65, 485–491.

Jones, N.P., Fournier, J.C., Stone, L.B., 2017. Neural correlates of autobiographical problem-solving deficits associated with rumination in depression. J. Affect. Disord. 218, 210–216.

Korgaonkar, M.S., Grieve, S.M., Etkin, A., Koslow, S.H., Williams, L.M., 2013. Using standardized fMRI protocols to identify patterns of prefrontal circuit dysregulation that are common and specific to cognitive and emotional tasks in major depressive disorder: first wave results from the iSPOT-D study. Neuropsychopharmacology 38, 863–871.

Krishnan, A., Williams, L.J., McIntosh, A.R., Abdi, H., 2011. Partial least squares (PLS) methods for neuroimaging: a tutorial and review. NeuroImage 56, 455–475.

Lee, L., Harkness, K.L., Sabbagh, M.A., Jacobsen, J.A., 2005. Mental state decoding abilities in clinical depression. J. Affect. Disord. 86, 247–258.

Lin, F.H., McIntosh, A.R., Agnew, J.A., Eden, G.F., Zeffiro, T.A., Belliveau, J.W., 2003. Multivariate analysis of neuronal interactions in the generalized partial least squares

framework: simulations and empirical studies. NeuroImage 20, 625–642.
McIntosh, A.R., Lobaugh, N.J., 2004. Partial least squares analysis of neuroimaging data: applications and advances. NeuroImage 23, S250–S263.
McTeague, L.M., Goodkind, M.S., Etkin, A., 2016. Transdiagnostic impairment of cognitive control in mental illness. J. Psychiatr. Res. 83, 37–46.
McTeague, L.M., Huemer, J., Carreon, D.M., Jiang, Y., Eickhoff, S.B., Etkin, A., 2017. Identification of common neural circuit disruptions in cognitive control across psychiatric disorders. Am. J. Psychiatry 174, 676–685.
Milan, L., Whittaker, J., 1995. Application of the parametric bootstrap to models that incorporation a singular value decomposition. J. R. Stat. Soc., Ser. C, Appl. Stat. 44, 31–49.
Mohn, C., Rund, B.R., 2016. Significantly improved neurocognitive function in major depressive disorders 6 weeks after ECT. J. Affect. Disord. 202, 10–15.
Muthén, L.K., Muthén, B.O., 1998-2017. Mplus User's Guide, Eighth edition. Muthén & Muthén, Los Angeles, CA.
Myerson, J., Green, L., Warusawitharana, M., 2001. Area under the curve as a measure of discounting. J. Exp. Anal. Behav. 76, 235–243.
Neale, M.C., Cardon, L.R., 1992. Methodology for Genetic Studies of Twins and Families. Kluwer Academic, Dordrecht, the Netherlands.
Opel, N., Redlich, R., Grotegerd, D., Dohm, K., Zaremba, D., Meinert, S., ... Dannlowski, U., 2017. Prefrontal brain responsiveness to negative stimuli distinguishes familial risk for major depression from acute disorder. J. Psychiatry Neurosci. 42, 343–352.
Palombo, D.J., Sheldon, S.M., Levine, B., 2018. Individual differences in autobiographical memory. Trends Cogn. Sci. 22, 583–597.
Power, J.D., Cohen, A.L., Nelson, S.M., Wig, G.S., Barnes, K.A., ... Petersen, S.E., 2011. Functional network organization of the human brain. Neuron 72, 665–678.
Power, J.D., Barnes, K.A., Snyder, A.Z., Schlaggar, B.L., Petersen, S.E., 2012. Spurious but systematic correlations in functional connectivity MRI networks arise from subject motion. NeuroImage 59, 2142–2154.
Power, J.D., Schlaggar, B.L., Petersen, S.E., 2015. Recent progress and outstanding issues in motion correction in resting state fMRI. NeuroImage 105, 536–551.
Ramirez-Mahaluf, J., Roxin, A., Mayberg, H.S., Compte, A., 2017. A computational model of major depression: the role of glutamate dysfunction on cingulo-frontal network dynamics. Cereb. Cortex 27, 660–679.
Rayner, G., Jackson, G., Wilson, S., 2016. Cognition-related brain networks underpin the symptoms of unipolar depression: evidence from a systematic review. Neurosci. Biobehav. Rev. 61, 53–65.
Ristow, I., Li, M., Colic, L., Marr, V., Födisch, C., von Düring, F., ... Walter, M., 2018. Pedophilic sex offenders are characterised by reduced GABA concentration in dorsal anterior cingulate cortex. NeuroImage 18, 335–341.
Rose, E.J., Ebmeier, K.P., 2006. Pattern of impaired working memory during major depression. J. Affect. Disord. 90, 149–161.
Rubinov, M., Sporns, O., 2010. Complex network measures of brain connectivity: uses and interpretations. NeuroImage 52, 1059–1069.
Rubinov, M., Sporns, O., 2011. Weight-conserving characterization of complex functional brain networks. NeuroImage 56, 2068–2079.
Sackeim, H.A., 2014. Autobiographical memory and electroconvulsive therapy: do not throw out the baby. J. ECT 30, 177–186.
Sackeim, H.A., Prudic, J., Nobler, M.S., Fitzsimons, L., Lisanby, S.H., Payne, N., Devanand, D.P., 2008. Effects of pulse width and electrode placement on the efficacy and cognitive effects of electroconvulsive therapy. Brain Stimulation 1 (2), 71–83.
Satterthwaite, T.D., Wolf, D.H., Ruparel, K., Erus, G., Elliott, M.A., Eickhoff, S.B., Gennatas, E.D., Jackson, C., Prabhakaran, K., Smith, A., Hakonarson, H., Verma, R., Davatzikos, C., Gur, R.E., Gur, R.C., 2013. Heterogeneous impact of motion on fundamental patterns of developmental changes in functional connectivity during youth. NeuroImage 83, 45–57.
Satterthwaite, T.D., Wolf, D.H., Roalf, D.R., Ruparel, K., Erus, G., Vandekar, S., ... Gur, R.C., 2015. Linked sex differences in cognition and functional connectivity in youth. Cereb. Cortex 25 (9), 2383–2394.
Schneider, D., Regenbogen, C., Kellermann, T., Finkelmeyer, A., Kohn, N., Derntl, B., ... Habel, U., 2012. Empathic behavioral and physiological responses to dynamic stimuli in depression. Psychiatry Res. 200, 294–305.
Seeley, W.W., Menon, V., Schatzberg, A.F., Keller, J., Glover, G.H., Kenna, H., Reiss, A.L., Greicius, M.D., 2007. Dissociable intrinsic connectivity networks for salience processing and executive control. J. Neurosci. 27, 2349–2356.
Semkovska, M., McLoughlin, D.M., 2010. Objective cognitive performance associated with electroconvulsive therapy for depression: a systematic review and meta-analysis. Biol. Psychiatry 68, 568–577.
Semkovska, M., McLoughlin, D.M., 2014. Retrograde autobiographical amnesia after electroconvulsive therapy: on the difficulty of finding the baby and clearing murky bathwater. J. ECT 30, 187–188.
Sheldon, S., Farb, N., Palombo, D.J., Levine, B., 2016. Intrinsic medial temporal lobe connectivity relates to individual differences in episodic autobiographical remembering. Cortex 74, 206–216.
Sherry, A., Henson, R.K., 2005. Conducting and interpreting canonical correlation analysis in personality research: a user-friendly primer. J. Pers. Assess. 84, 37–48.
Smith, A., 1982. Symbol Digit Modalities Test-Revised. Western Psychological Services, Los Angeles.
Smith, S.M., Jenkinson, M., Woolrich, M.W., Beckmann, C.F., Behrens, T.E.J., ... Matthews, P.M., 2004. Advances in functional and structural MR image analysis and implementation as FSL. NeuroImage 23, 208–219.
Smith, S.M., Beckmann, C.F., Andersson, J., Auerbach, E.J., Bijsterbosch, J., Douaud, G., Duff, E., Feinberg, D.A., Griffanti, L., Harms, M.P., Kelly, M., Laumann, T., Miller, K.L., Moeller, S., Petersen, S., Power, J., Salimi-Khorshidi, G., Snyder, A.Z., Vu, A.T., Woolrich, M.W., et al., 2013. Resting-state fMRI in the human connectome project. Neuroimage 80, 144–168.
Smith, R., Keramatian, K., Christoff, K., 2007. Localizing the rostrolateral prefrontal cortex at the individual level. Neuroimage 36, 1387–1396.
Smith, S.M., Nichols, T.E., Vidaurre, D., Winkler, A.M., Behrens, T.E.J., Glasser, M.F., ... Miller, K.L., 2015. A positive-negative mode of population covariation links brain connectivity, demographics and behavior. Nat. Neurosci. 18, 1565–1567.
Söderlund, H., Moscovitch, M., Kumar, N., Mandic, M., Levine, B., 2012. As time goes by: hippocampal connectivity changes with remoteness of autobiographical memory retrieval. Hippocampus 22, 670–679.
Söderlund, H., Percy, A., Levine, B., 2012. Electroconvulsive therapy for depression and autobiographical memory. In: Zeman, A., Kapur, N., Jones-Gotman, M. (Eds.), Epilepsy and Memory. Oxford Scholarship Online: Oxford University Press.
Söderlund, H., Moscovitch, M., Kumar, N., Daskalakis, Z.J., Flint, A., Herrmann, N., Levine, B., 2014. Autobiographical episodic memory in major depressive disorder. J. Abnorm. Psychol. 123, 51–60.
Sporns, O., Betzel, R.F., 2016. Modular brain networks. Annu. Rev. Psychol. 67, 613–640.
Spreng, R.N., Stevens, W.D., Chamberlain, J.P., Gilmore, A.W., Schacter, D.L., 2010. Default network activity, coupled with the frontoparietal control network, supports goal-directed cognition. NeuroImage 53, 303–317.
Spreng, R.N., DuPre, E., Selarka, D., Garcia, J., Gojkovic, S., Mildner, J., ... Turner, G.R., 2014. Goal-congruent default network activity facilitates EF. J. Neurosci. 34, 14108–14114.
Sridharan, D., Levitin, D.J., Menon, V., 2008. A critical role for the right frontoinsular cortex in switching between central-executive and default-mode networks. Proc. Natl. Acad. Sci. USA. 105, 12569–12574.
Tsvetanov, K.A., Henson, R.N.A., Tyler, L.K., Razi, A., Geerligs, L., Ham, T.E., Rowe, J.B., 2016. Extrinsic and intrinsic brain network connectivity maintains cognition across the lifespan despite accelerated decay of regional brain activation. J. Neurosci. 36, 3115–3126.
Van Dijk, K.R., Sabuncu, M.R., Buckner, R.L., 2012. The influence of head motion on intrinsic functional connectivity MRI. Neuroimage 59, 431–438.
Van Essen, D.C., Ugurbil, K., Auerbach, E., Barch, D., Behrens, T.E., Bucholz, R., Chang, A., Chen, L., Corbetta, M., Curtiss, S.W., Della Penna, S., Feinberg, D., Glasser, M.F., Harel, N., Heath, A.C., Larson-Prior, L., Marcus, D., Michalareas, G., Moeller, S., Oostenveld, R., et al., 2012. The Human Connectome Project: a data acquisition perspective. Neuroimage 62, 2222–2231.
Vannucci, M., Pelagatti, C., Chiorri, C., Mazzoni, G., 2016. Visual object imagery and autobiographical memory: object imagers are better at remembering their personal past. Memory 24, 455–470.
Vatansever, D., Menon, D.K., Manktelow, A.E., Sahakian, B.J., Stamatakis, E.A., 2015. Default mode dynamics for global functional integration. J. Neurosci. 35, 15254–15262.
Vatansever, D., Bzdok, D., Wang, H., Mollo, G., Sormaz, M., Murphy, C., ... Jefferies, E., 2017. Varieties of semantic cognition revealed through simultaneous decomposition of intrinsic brain connectivity and behaviour. NeuroImage 158, 1–11.
Verhulst, B., 2017. A power calculator for the classical twin design. Behav. Genet. 47, 255–261.
Watkins, E.R., Nolen-Hoeksema, S., 2014. A habit-goal framework of depressive rumination. J. Abnorm. Psychol. 123, 24–34.
Westphal, A.J., Wang, S., Rissman, J., 2017. Episodic memory retrieval benefits from a less modular brain network organization. J. Neurosci. 37, 3523–3531.
Wheatley, T., Milleville, S.C., Martin, A., 2007. Understanding animate agents: distinct roles for the social network and mirror system. Psychol. Sci. 18, 469–474.
Whitfield-Gabrieli, S., Nieto-Castanon, A., 2012. CONN: a functional connectivity toolbox for correlated and anticorrelated brain networks. Brain Connect. 2, 125–141.
Whitmer, A.J., Gotlib, I.H., 2013. An attentional scope model of rumination. Psychol. Bull. 139, 1036–1061.
Yang, Z., Zuo, X., McMahon, K.L., Craddock, R.C., Kelly, C., de Zubicaray, G.I., ... Wright, M.J., 2016. Genetic and environmental contributions to functional connectivity architecture of the human brain. Cereb. Cortex 26, 2341–2352.
Yeo, B.T.T., Krienen, F.M., Sepulcre, J., Sabuncu, M.R., Lashkari, D., Hollinshead, M., ... Buckner, R.L., 2011. The organization of the human cerebral cortex estimated by intrinsic functional connectivity. J. Neurophysiol. 106, 1125–1165.
Zakzanis, K.K., Leach, L., Kaplan, E., 1998. On the nature and pattern of neurocognitive function in major depressive disorder. Neuropsychiatry Neuropsychol. Behav. Neurol. 11, 111–119.